Palaeogeography, Palaeoclimatology, Palaeoecology 520 (2019) 188–202

Contents lists available at ScienceDirect

Palaeogeography, Palaeoclimatology, Palaeoecology

journal homepage: www.elsevier.com/locate/palaeo

Middle–Upper Ordovician (Darriwilian–Sandbian) paired carbon and sulfur isotope stratigraphy from the Appalachian Basin, USA: Implications for dynamic redox conditions spanning the peak of the Great Ordovician Biodiversification Event

Nevin P. Kozik[a,*], Seth A. Young[a], Chelsie N. Bowman[a], Matthew R. Saltzman[b], Theodore R. Them II[c]

[a] Department of Earth, Ocean, and Atmospheric Science and National High Magnetic Field Laboratory, Florida State University, Tallahassee, FL 32306, USA
[b] School of Earth Sciences, The Ohio State University, Columbus, OH 43210, USA
[c] College of Charleston, Department of Geology and Environmental Geosciences, SC 29412, USA

ARTICLE INFO

Keywords:
Oxygenation
Biodiversification
Strontium isotopes
Chemostratigraphy
Paleoredox
Sea level

ABSTRACT

The Evans Ferry section from the Appalachian Basin of eastern North America has been analyzed for chemostratigraphic trends to elucidate possible causal mechanisms facilitating the Great Ordovician Biodiversification Event (GOBE). Paired stable isotope ($\delta^{13}C$ and $\delta^{34}S$) analyses were used in this carbonate-dominated locality from the Appalachian Basin to reconstruct the marine redox states during this key period of rapid biodiversification. This succession is one of the most expanded Sandbian Stage (Upper Ordovician) deposits known from North America, and it allows new high-resolution reconstructions of long-term, global carbon and sulfur cycle fluctuations. The integrated geochemical and sequence-stratigraphic investigation presented here from the Laurentian epeiric seaway allows for possible identification of the contraction and expansion of reducing water masses during the Middle–Late Ordovician that may have been linked to global-marine paleoredox dynamics. Utilizing new conodont-based $^{87}Sr/^{86}Sr$ isotope stratigraphy along with previous conodont biostratigraphy, we can confidently correlate our stable isotope profiles to other carbonate successions globally. Carbonate facies indicate that this area experienced partial restriction from open-marine conditions during certain intervals in the Sandbian. These semi-restricted environments record carbon ($\delta^{13}C_{carb}$) isotope trends that are secular in nature, as they can be correlated to other successions across Laurentia and Baltica. We identify several intervals when $\delta^{13}C_{carb}$ and $\delta^{34}S_{CAS}$ (carbonate-associated sulfate) trends are decoupled. These inverse stratigraphic trends are, at times, followed by parallel positive shifts in $\delta^{13}C_{carb}$ and $\delta^{34}S_{CAS}$. Causal mechanisms for the observed decoupled $\delta^{13}C$ and $\delta^{34}S$ trends may include a wide variety of factors such as more closed-system, local biogeochemical processes associated in part with diagenesis, or they could instead reflect variations in the global fluxes of organic matter and pyrite burial linked to changing marine paleoredox conditions. The positive covariation in trends presented here likely represents transient increases in organic carbon and pyrite burial in response to expansion of reducing marine environments.

1. Introduction

The Great Ordovician Biodiversification Event (GOBE) was the second of two immense radiations of marine fauna in the Paleozoic; the first occurred during the early Cambrian (i.e., Cambrian Explosion) and was associated with the evolution of most major body plans. The GOBE occurred during the Early to Middle Ordovician (~25–30-Myr in duration) and was associated with a significant diversification at lower taxonomic levels (Sepkoski et al., 1981; Droser and Sheehan, 1997; Peters, 2004). It represented a continuous rise in faunal diversity that is hypothesized to have been a continuation of the Cambrian Explosion after a brief hiatus in diversification (Droser and Finnegan, 2003). The GOBE was the largest radiation of marine fauna in the Phanerozoic with an approximate threefold increase in family-level diversity and twofold increase in generic diversity (Droser and Finnegan, 2003). The majority of planktonic diversification began in the early Dapingian, while major

* Corresponding author.
E-mail address: npk15@my.fsu.edu (N.P. Kozik).

https://doi.org/10.1016/j.palaeo.2019.01.032
Received 1 August 2018; Received in revised form 25 January 2019; Accepted 28 January 2019
Available online 02 February 2019
0031-0182/

diversification of benthic organisms was delayed until the early Sandbian (Servais et al., 2010). By the late Sandbian-early Katian stages, marine biodiversity had plateaued and was eventually followed by the first of the "Big 5" mass extinction events during the Hirnantian Stage (Harper et al., 2014).

Several hypotheses have been put forth to explain Ordovician biodiversification. It was proposed that, during the early Darriwilian, several large asteroid breakup events in a relatively short interval (roughly 467–465 Ma) caused habitat fragmentation which would have fueled biodiversification (Schmitz et al., 2008). The timing between the asteroid breakups and marine biodiversification has recently been called into question, however, as new radiometric dates from zircons within the meteorite-bearing beds reveal that the diversification began before the first sedimentary evidence of extraterrestrial chromite grains (Lindskog et al., 2017). Another hypothesis for the cause of the GOBE was global cooling of the upper ocean, which plummeted from a seemingly-uninhabitable 40 °C at low latitudes into habitable ranges of modern tropical sea surface temperatures of ~32 to 28 °C. This decrease in temperature was linked to an increased abundance of carbonate-calcifying marine organisms, which may have decreased atmospheric pCO_2 and affected climate (Trotter et al., 2008).

Another hypothesis focuses on the Taconic Orogeny, which spans the Middle–Late Ordovician and impacted the eastern margin of Laurentia (Fig. 1) and may have increased nutrient fluxes to the oceans via enhanced weathering of Laurentia. Enhanced weathering in the Taconic highlands would have delivered essential macro- and micronutrients (e.g., phosphorus and iron) to the oceans, thus drawing down atmospheric CO_2 through primary production and burial of organic matter (Cárdenas and Harries, 2010). Additionally, the increased weathering flux to continental margins would have changed the substrate that benthic organisms anchored to, resulting in ecological community shifts and fueling adaptation and diversification (Miller and Mao, 1995). Furthermore, the GOBE has been linked to an increase in the oxygen content of the global oceans, as more ventilated oceanic conditions would have been more conducive to the expansion of marine faunas (Knoll and Carroll, 1999). Thus, progressive oxygenation of deep shelf and slope regions would have provided new habitat/niche spaces where marine organisms could expand (Stanley, 1973; Sperling et al., 2013). Oceanic oxygenation has been previously linked to diversification events in the Neoproterozoic that allowed for the rise in soft-bodied Ediacarian fauna and acanthomorph acritarchs (e.g., Fike et al., 2006; Canfield et al., 2007; Johnston et al., 2012). Oxygenation has also been recently linked to the GOBE through carbon-sulfur mass balance models, which utilize high-resolution carbon isotope records (Edwards et al., 2017).

Early Paleozoic chemostratigraphic studies of paired carbon and sulfur isotopes are integral to our basic understanding of changes in the long-term carbon and sulfur cycles, and key to reconstructions of marine redox environments (Thompson and Kah, 2012; Saltzman et al., 2015). Stable isotopes of carbon and sulfur have been used throughout the geologic record to document and correlate perturbations in the carbon cycle with major biotic events such as the GOBE (Korte et al., 2004; Saltzman et al., 2011; Chen et al., 2013; Jones and Fike, 2013; Young et al., 2016). Long-term carbon and sulfur cycles are linked through the oxidation of organic matter produced by photosynthetic organisms through the anaerobic microbial pathway of sulfate reduction (Berner, 2004). The marine sulfate reservoir is coupled to atmospheric pO_2 levels, as the main flux of sulfate into the oceans (i.e., riverine) is mediated by the oxidative weathering of pyrite and other sulfide minerals on land. Microbial processes may reduce the available sulfate and produce H_2S as a waste product, which readily bonds with reduced iron (Fe^{2+}) to form pyrite (Canfield et al., 1992). Studies of paired carbon and sulfur isotopes allow inferences to be drawn about the linkages, timing, and feedbacks that drove major perturbations in these important elemental cycles (e.g., Gill et al., 2011; Saltzman et al., 2011; Owens et al., 2013). This information is paramount in assessing the overall importance of marine redox conditions to this key marine radiation event during the Ordovician.

Most studies during the Ordovician have primarily used carbon isotope stratigraphy to elucidate changes in the carbon cycle (Saltzman, 2005; Munnecke et al., 2010; Edwards and Saltzman, 2015), and in comparison, there are relatively few sulfur isotope studies. These sulfur-isotope studies have been focused mainly on specific intervals within the Tremadocian and Darriwilian stages (e.g., Thompson and Kah, 2012; Marenco et al., 2013; Young et al., 2016; Edwards et al., 2018), and few sulfur isotope studies have ranged into the Sandbian Stage, when marine taxa continued to diversify. Here, we present high-resolution datasets of paired carbon and sulfur isotopes from an expanded section of Middle–Upper Ordovician carbonates, and we use box model simulations to explore possible drivers of the observed stable isotopic trends such as paleoredox, weathering, biotic fractionation, and diagenesis.

2. Background

2.1. Geologic setting

The study site was located along the eastern margin of the paleocontinent Laurentia during the Middle-Late Ordovician (Fig. 1), specifically within the foreland basin that formed as a result of the ongoing Taconic Orogeny (e.g., Ettensohn and Lierman, 2012). The onset of foreland basin formation in this area is marked stratigraphically by the Knox Unconformity, which is thought to represent the transition from a passive to an active margin in eastern Laurentia, and can be correlated throughout the Appalachian Basin (Mussman and Read, 1986). The studied section is located approximately 35 miles north of Morristown, Tennessee, along US highway 25E within the Valley and Ridge Province of the Appalachian Mountains (36°23′15.1″ N 83°26′51.1″ W).

The Evans Ferry roadcut exposes the lower-middle portions of the Chickamauga Group, which contains six formations that lie unconformably above the Knox Dolomite (Figs. 2A, 3; Pope and Read, 1998). The basal unit of this section is the Five Oaks Formation (Fm.), a carbonate mudstone with several intervals of skeletal wackestone-packstone that contain the following: bryozoan, brachiopods, trilobites, crinoids, and occasional tabulate and rugose corals. This formation also contains distinctive chert-rich intervals that, in some horizons, form meter-long nodules. Overlying the Five Oaks Fm. is the Lincolnshire Fm., which consists predominantly of interbedded packstone and calcareous shale. The packstone interbeds (Fig. 2F) contain fragmented brachiopods, bryozoans, and crinoids with occasional trilobites, orthocone cephalopods, and sponges. The Rockdell Formation overlies the Lincolnshire and is a massively bedded lime mudstone that contains well-preserved, in situ skeletal remains of stromatoporoids, orthocone cephalopods, branching bryozoans, and tabulate corals (Fig. 2B). The overlying Benbolt Fm. has a similar lithologic and skeletal composition to the Lincolnshire Fm., and consists of interbedded packstone and calcareous shale. The Benbolt Fm. is overlain by the Wardell Formation, which is primarily composed of massively bedded packstone with very fine siltstone laminations. Within this formation, there are two major stratigraphic horizons of dolostone that contain abundant pink crinoid stem fragments and stylolites. The Witten Fm. is the youngest formation exposed at the Evans Ferry locality. It has a basal shale that contains minor graptolite fragments, overlain by massively bedded micrite (Fig. 2I) with occasional brachiopods and bryozoans. Near the top of the formation, bedding becomes thin and mud cracks (Fig. 2C), ripple marks, and oncoids (Fig. 2H) are common. The top of our measured section is marked by a major thrust fault within the upper Witten Formation.

A previous study has published conodont biostratigraphy at this locality, and although very few diagnostic conodonts were recovered from this sequence, the fauna suggests that the strata were deposited during the Darriwilian through Sandbian stages (Bergström and Carnes,

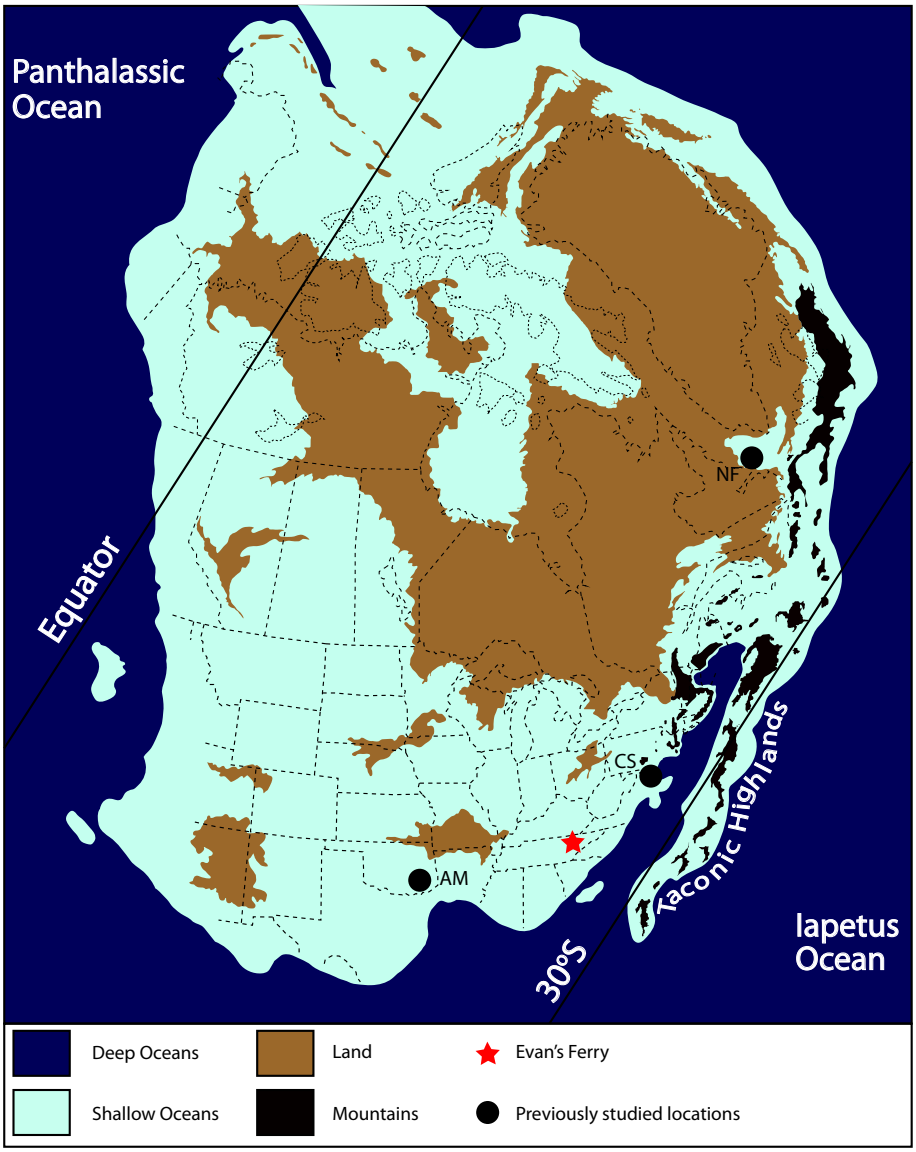

Fig. 1. Middle-Late Ordovician paleogeographic map. Modified from Blakey (2011) with the locations of other study areas show in black circles. The Evans Ferry section (this study, red star) is located on the Laurentian craton side of the Appalachian Foreland Basin. AM = Arbuckle Mountains; CS = Clear Springs; NF = Western Newfoundland. (For interpretation of the references to color in this figure legend, the reader is referred to the web version of this article.)

1985). The Five Oaks and Lincolnshire formations contain conodont elements indicative of the *Cahabagnathus sweeti* Midcontinent Biozone, which overlaps with the upper portion of the *Pygodus anserinus* to lower *Amorphognathus tvaerensis* North Atlantic Conodont Biozones (Bergström and Carnes, 1985; Carnes, 1975). The Rockdell and Benbolt formations contain a conodont fauna interpreted to be within the *Baltoniodus gerdae* Subzone of the *Amorphognathus tvaerensis* North Atlantic Conodont Biozone (Carnes, 1975). The strata at Evans Ferry can be correlated to a succession in nearby Thorn Hill, Tennessee, which is within the next thrust sheet to the northeast of Evans Ferry (Bergström and Carnes, 1985). The Thorn Hill section contains conodont fauna (i.e., North Atlantic biozones) and sedimentary facies indicative of deeper-water environments compared to that of the Evans Ferry section (Bergström and Carnes, 1985), although that outcrop is now mostly covered. The Witten Fm. at Evans Ferry is biostratigraphically poorly constrained due to low and non-diagnostic conodont yields. The Moccasin Fm. overlies the Witten Fm. at the Thorn Hill section, and the Deicke and Millbrig K-bentonite ash beds have been identified in this stratigraphic unit (Haynes, 1994). This implies that the Evans Ferry site must be older than the *P. undatus* Midcontinent Conodont Zone where these well-studied, widespread K-bentonite beds are located (e.g., Kolata et al., 1996). Thus, the upper Witten Fm. at Evans Ferry is likely within the *B. compressa* Midcontinent or equivalent portion of the *B. alobatus* North Atlantic conodont biozones.

2.2. Carbon and sulfur biogeochemical cycles

Stratigraphic intervals with significantly positive $\delta^{13}C$ values ($> +2‰$ magnitude, $\delta^{13}C_{carb}$ and $\delta^{13}C_{org}$) have been traditionally interpreted to reflect increased global primary productivity and carbon burial (Kump and Arthur, 1999). As primary producers consume dissolved inorganic carbon (DIC) during photosynthesis, they preferentially incorporate isotopically light carbon (^{12}C) during organic matter (OM) production. When this organic matter sinks from the surface ocean to the seafloor, it is either remineralized or buried. The stable isotopic signature of the global seawater DIC pool, preserved as carbonate carbon isotopes ($\delta^{13}C_{carb}$), becomes progressively heavier over time as more ^{12}C is buried as OM (Kump and Arthur, 1999). As primary producers assimilate DIC from an increasingly isotopically heavier reservoir during OM production, which then can be exported to

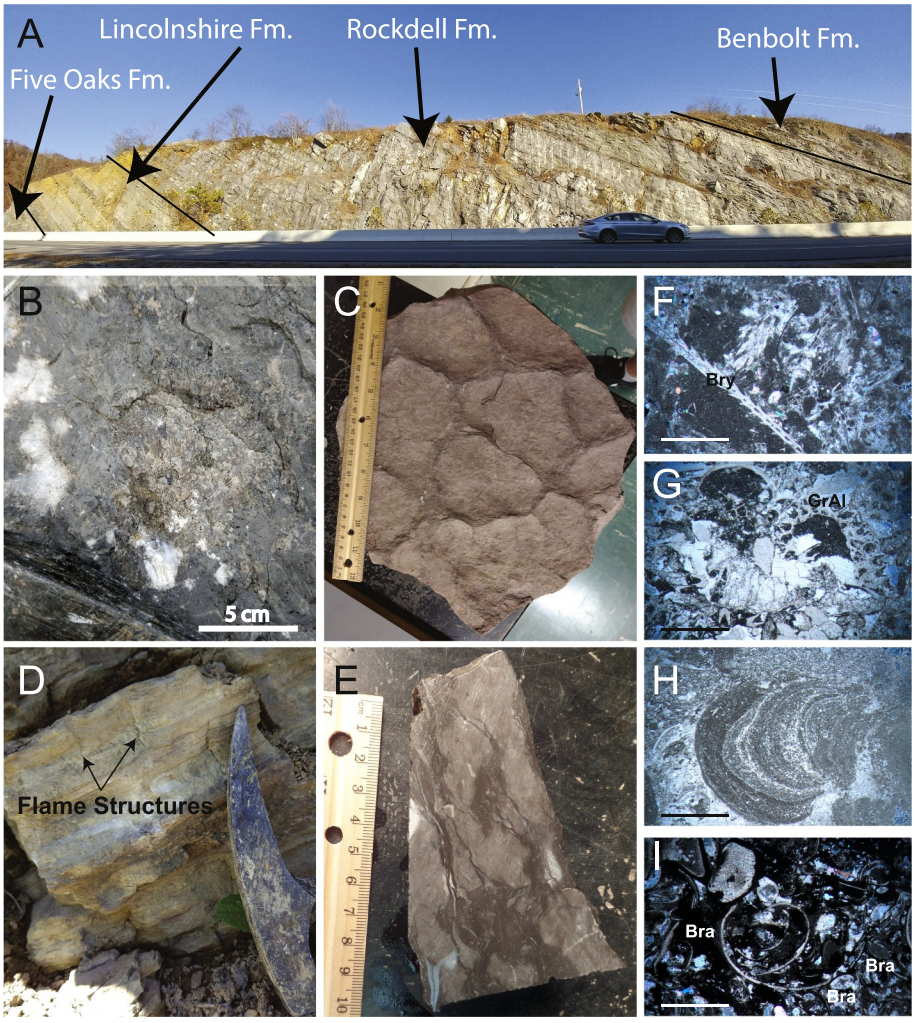

Fig. 2. Outcrop photos and thin section photomicrographs from Evans Ferry, TN. A) Lower and Middle Chickamauga Group exposed along highway US 25 near Evans Ferry, TN. B) Large tabulate coral within a bioherm from the Rockdell Fm. C) Desiccation cracks within the upper Witten Fm. D) Flame structure within the upper Witten. E) Polished surface of the Middle Five Oaks Fm. F) Photomicrograph of large bryozoan (Bry) found within the Five Oaks Fm. G) Photomicrograph of calcareous green algae (GrAl) found within the bioherm from the Rockdell Fm. H) Coated grain, an oncoid from the upper Witten Fm. I) Brachiopod (Bra) packstone with phosphate replaced lime mud within the lower Witten Fm. All scale bars in panels D–I are 1.5 mm.

the seafloor and buried, it is also possible to track these changes using bulk organic carbon isotopes ($\delta^{13}C_{org}$). The photosynthetic fractionation factor (ε_p) between the isotopic composition of the DIC reservoir and exported organic carbon is not thought to be constant over time or necessarily across different phytoplankton groups, and this can also influence $\delta^{13}C$ records (Hayes et al., 1999). The difference in carbonate and organic carbon isotopes from the same sample, displayed as $\Delta^{13}C$ ($\Delta^{13}C = \delta^{13}C_{carb} - \delta^{13}C_{org}$), can allow for the approximation of ε_p from the rock record, which can then be used to reconstruct relative changes in atmospheric pCO_2 at the time of deposition (Berner et al., 2000). Variations in pCO_2 can affect the efficacy of carbon fixation in the enzyme Rubisco, which can have an effect on ε_p (Young et al., 2008; Edwards et al., 2017). Furthermore, if ε_p can be estimated, the relative changes in pCO_2, as well as pO_2, can be inferred (Edwards et al., 2017). Changes in silicate weathering rates may also significantly impact the long-term carbon cycle, specifically the rapid weathering of basaltic volcanic rocks, which consumes CO_2 (Berner, 2006a, 2006b). This study will focus on the production and burial of organic matter, silicate/carbonate weathering, and the $\Delta^{13}C$ of the long-term carbon cycle as the primary drivers for the perturbations observed within the previously described study site.

Similar to carbon, sulfur is isotopically fractionated as microbes preferentially use the lighter isotopes of sulfur in their metabolisms (e.g., sulfate reduction). Sulfate (SO_4^{2-}), one of the most abundant dissolved ions in modern oceans, is used as the terminal electron acceptor in microbial sulfate reduction (MSR). Most sulfate reducers require organic matter as a substrate, which is supplied by primary producers (Mitterer, 2010). The by-product of MSR is hydrogen sulfide (H_2S), which readily reacts with any available iron within the water column or sediments, ultimately forming pyrite (FeS_2):

$$2Fe_2O_3 + 8SO_4^{2-} + 16H^+ + CH_2O \rightarrow 15O_2 + 4FeS_2 + CO_2 + 9H_2O \quad (1)$$

If increased amounts of pyrite are buried above background levels, then it has the ability to change the global sulfur-isotopic composition of the marine sulfate reservoir (e.g., Lyons and Gill, 2010; Berner, 2006a, 2006b). An increase in MSR and/or increased preservation of pyrite within the sediments (i.e., reduction in the rate of re-oxidation of this reduced sulfur pool) can result in a positive sulfur isotope ($\delta^{34}S$) excursion of sulfate and/or sedimentary pyrite. Similar to the burial of organic carbon, pyrite burial also creates free oxygen as a byproduct. Therefore, long-term changes in the burial flux of pyrite in sediments may also lead to changes in the long-term flux of oxygen to the ocean-atmosphere system (Berner, 2001, 2006a, 2006b; Wildman et al., 2004). The formation and oxidation of pyrite is one of the largest controls on atmospheric pO_2 levels on geologic time scales; the oxidation of pyrite consumes O_2 and the burial of pyrite releases O_2 (Lyons and Gill, 2010). Secular changes in the sulfur isotope composition of the global seawater sulfate pool can be tracked using the carbonate-associated sulfate (CAS) sulfur isotope proxy ($\delta^{34}S_{CAS}$), which responds to global changes in pyrite burial. $\delta^{34}S_{CAS}$ records record the global sulfur isotopic composition of seawater sulfate at the time of carbonate formation because the sulfate ion easily substitutes into the calcite crystal lattice for bicarbonate/carbonate ion with minimal fractionation

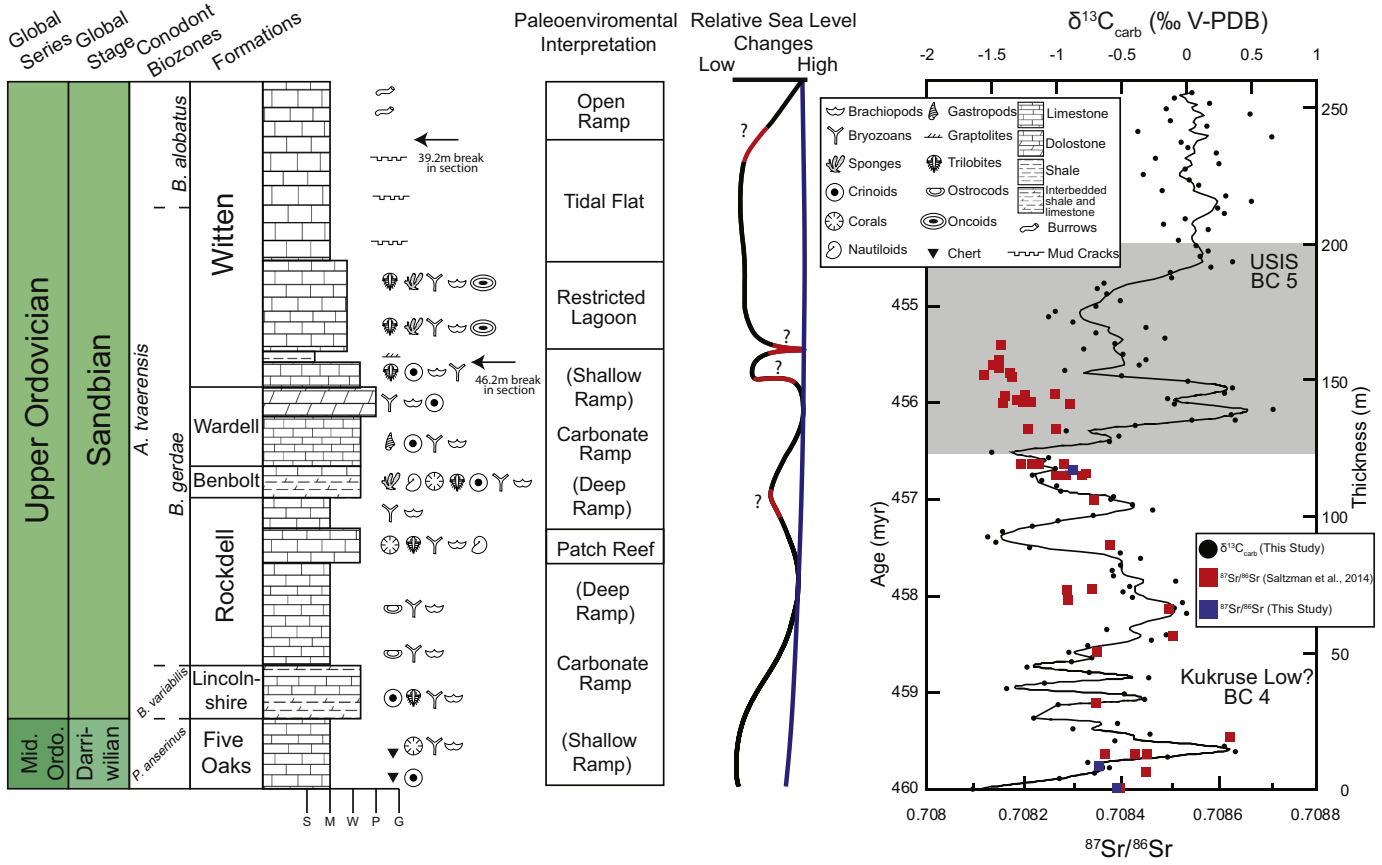

Fig. 3. Generalized lithologic column and facies interpretations for the Evans Ferry, TN study section, with new $\delta^{13}C_{carb}$ chemostratigraphy (black circles), $^{87}Sr/^{86}Sr$ ratios (red and blue squares). Generalized sea-level curve was produced through sequence stratigraphic analysis, reveals three third order sea-level cycles (black line) superimposed over a transgressive second order sea-level curve (modified from Haq and Schutter, 2008). Red intervals on the sea-level curve indicate portions of missing sea-level cycles either not preserved or removed through anthropogenic means. Absolute ages are based on the calibrated Strontium Isotope Stratigraphy (SIS) from Saltzman et al. (2014). Facies interpretation are based on lithofacies analyses, thin sections, and sedimentary structures found within the section. Arrows denoting section breaks are due to two roads which separate otherwise continuous roadcut exposure. Conodont biozones are after Bergström and Carnes (1985) and inferred from new conodont-apatite based SIS presented here. Note that black line within $\delta^{13}C_{carb}$ values is a smoothed 3-pt weighted running average. S = shale; M = mudstone; W = wackestone; P = packstone; G = grainstone. (For interpretation of the references to color in this figure legend, the reader is referred to the web version of this article.)

(Burdett et al., 1989). Meanwhile, $\delta^{34}S$ of sedimentary pyrite ($\delta^{34}S_{pyr}$) is used as a proxy for local changes in MSR and redox conditions. This is because pyrite formation is controlled by several factors that vary locally, such as availability of Fe^{2+}, availability/type of organic matter, and rates of MSR (Gill et al., 2008; Leavitt et al., 2013).

3. Materials and methods

3.1. Stratigraphic analysis and sample preparation

Lithologic samples were collected from the Evans Ferry roadcut at ~1 m intervals. Stratigraphic horizons with extensive recrystallization, secondary calcite veins, and/or pyrite nodules were avoided. Weathered portions of samples were mechanically removed using a diamond blade saw. Small slabs were cut and used to create thin section billets, and approximately 1 g of powder was microdrilled from micritic matrix for $\delta^{13}C_{carb}$ analysis. The remaining samples were powdered using a SPEX 8510 ShatterBox, and splits of these powders were taken for $\delta^{13}C_{org}$ and $\delta^{34}S_{CAS}$ analyses. Three previously collected conodont samples from the same stratigraphic section at Evans Ferry were chosen for $^{87}Sr/^{86}Sr$ analysis from archived conodont collections that yielded 0.1–0.7 mg of whole and broken conodont elements with CAI values ~4 (Carnes, 1975).

3.2. Stable isotopic analyses (C, O, S)

Between 100 and 300 µg of carbonate powder were weighed and then acidified with 3–5 drops of anhydrous phosphoric acid (H_3PO_4) at 25 °C for 24 h. Stable carbon and oxygen isotope ratios of the evolved CO_2 gas were measured using a Gas Bench II Autocarbonate device paired to a ThermoFinnigan Delta Plus XP stable isotope ratio mass spectrometer (IRMS) at the National High Magnetic Field Laboratory at Florida State University (NHMFL-FSU). All carbon and oxygen results are reported in standard delta-notation (δ) with units reported as per mil (‰) relative to the VPDB (Vienna Pee Dee Belemnite) standard for $\delta^{13}C$ and $\delta^{18}O$. The analytical precision for $\delta^{13}C$ and $\delta^{18}O$, based on long-term, replicate analysis of NBS-19 and our internal lab standards, is ± 0.05‰ and ± 0.1‰, respectively (1σ standard deviations). Internal standards include the following: $\delta^{13}C$ and $\delta^{18}O$ isotope values reported respectively to V-PDB: ROY-CC (+0.67‰, −12.02‰), MB-CC (−10.5‰, −3.5‰), and PDA (−1.3‰, −5.34‰).

For $\delta^{13}C_{org}$ analysis, approximately 5 g of sample powder were weighed and then reacted with 6 N HCl. Each sample was acidified and centrifuged three times to remove all carbonate minerals; the insoluble residues were then rinsed in ultrapure (deionized 18.2 MΩ) water until all HCl was removed; and then samples were placed in a 70 °C oven to dry overnight. The residues were homogenized, placed into tin capsules where their masses were recorded, and then analyzed by IRMS. The

carbon isotopic ratios of the samples were measured using a Carlo Erba Elemental Analyzer coupled to a ThermoFinnigan Delta Plus XP IRMS and combusted at 1020 °C. Sample precision and calibration of data are performed during routine analyses of laboratory standards that are calibrated against IAEA standards. Internal FSU standards include: Acetanilide (−29.2‰), Urea-2 (−8.13‰), and WYSTD (−12.7‰). The analytical precision for $\delta^{13}C_{org}$ is ± 0.2‰ and ± 0.7% for %C (1σ) or better. Weight percent of total organic carbon (TOC) in the samples is determined by comparison of voltages for the CO_2^+ ion beam intensities of masses 44, 45, and 46 between our samples and known wt% carbon of the gravimetric standard Acetanilide analyzed during the same sequence (e.g., Young et al., 2008). Uncertainties in calculated TOC percentages are better than ± 5%.

Carbonate-associated sulfate (CAS) extraction was carried out with only minor modifications to the procedures outlined by Wotte et al. (2012). Between 80 and 120 g of powder were weighed and then rinsed three times in 10% NaCl solution for 12 h. Following this, the samples were rinsed three times in ultrapure water for 12 h. Next, 6 N HCl was titrated into the samples for ≤2 h to dissolve all $CaCO_3$ and liberate sulfate from the carbonate matrix. The insoluble fractions were removed from the acidified solution via centrifugation. The acidified solution was then brought up to a pH of 10 using a NaOH solution. The precipitates from this reaction were removed from the remaining solution via vacuum filtration, and the solution was brought down to pH 4 using 12 N HNO_3. Excess saturated $BaCl_2$ solution was then added to all samples to precipitate the liberated CAS as barite ($BaSO_4$). This solution was allowed to precipitate for up to 72 h before the barite was rinsed in ultrapure water and dried overnight. Samples were then weighed into tin cups along with 2–5 mg of V_2O_5 for sulfur isotope analysis using a Thermo Isolink Elemental Analyzer coupled to a Thermo Delta V Plus IRMS via a Conflo-IV open split interface at the NHMFL-FSU. All sulfur isotope results are reported in standard delta-notation (δ) with units reported in per mil (‰) relative to V-CDT (Cañon Diablo Troilite). Samples are calibrated to internal laboratory standards EMR-CP (+0.9‰), PQM2 (−16‰), ERE (−4.7‰), PQB-D (+40.5‰), and SWP (+20.3‰) with standard deviations of ± 0.2‰ or better (one sigma1σ).

3.3. $^{87}Sr/^{86}Sr$ of conodont apatite

Approximately 0.1 to 0.7 mg of conodont elements were picked from each sample, excluding any that had any obvious signs of alteration or mineral overgrowths (see Saltzman et al., 2014), which are archived in the conodont collections at Ohio State University (Carnes, 1975). Samples were sonicated overnight with 1 mL of ultrapure water to remove any surficial contaminants and adhesives. Samples were then cleaned with ultrapure 1 M ammonium acetate (buffered to pH = 8). Once cleaned, all samples were dissolved in ultrapure 6 N HCl and spiked with an ^{84}Sr tracer, and purified through H^+ cation exchange resin through two elutions of 2 N HCl in silica glass columns (Foland and Allen, 1991). Measurements for $^{87}Sr/^{86}Sr$ were performed at the Radiogenic Isotope Laboratory in the School of Earth Sciences at Ohio State University. Values were obtained using a dynamic multicollector on a Finnigan MAT-261A thermal ionization mass spectrometer with a typical interarm precision of 0.000009 (2σ). All values were normalized for instrument fractionation using a normal Sr ratio of $^{86}Sr/^{88}Sr = 0.119400$.

4. Results

The $\delta^{13}C_{carb}$ record from the entire Chickamauga Group at the Evans Ferry road cut has an overall average value of −0.41‰ and a total range from −1.65 to +0.66‰ (Fig. 4A). In most of the Five Oaks to lower Witten formations, baseline $\delta^{13}C_{carb}$ values are approximately −0.75‰. There are several small-scale positive and negative shifts recorded in this interval, such as the +2.0‰ excursion in the Five Oaks (~15 m), the −1.2‰ shift in the upper Rockdell (~90 m), and the +1.2‰ shift in the Wardell/lower Witten interval (~140 m). In the middle Witten Formation there is a shift in baseline values from ~−1.0 to +0.5‰ (~175 to 195 m), and variation in the $\delta^{13}C_{carb}$ dataset is on an even smaller scale (< 0.5‰) above this change in baseline.

The $\delta^{13}C_{org}$ data show significantly more variability throughout the section, with a range from −31.7 to −21.8‰ (Fig. 4B). Baseline values in the $\delta^{13}C_{org}$ record are between −28 and −29‰ throughout the Evans Ferry roadcut. The most notable perturbations from the baseline all represent increased values, including: 1) a +5‰ excursion in the Five Oaks (~25 m); 2) a +8‰ excursion in the lower Witten (~165 m); and 3) a +5‰ excursion in the upper Witten (~210 m). Of these three notable positive $\delta^{13}C_{org}$ excursions, the $\delta^{13}C_{org}$ shift in the Five Oaks closely tracks the positive shift in $\delta^{13}C_{carb}$, whereas the $\delta^{13}C_{org}$ excursion in the lower Witten has no corresponding $\delta^{13}C_{carb}$ excursion. The $\delta^{13}C_{org}$ excursion in the upper Witten parallels a positive shift in $\delta^{13}C_{carb}$ baseline values. The $\Delta^{13}C$ values (Fig. 4C) largely mirror the $\delta^{13}C_{org}$ dataset, with only small-scale changes (on the order of 1–2‰) observed in the $\delta^{13}C_{carb}$ data.

The $\delta^{34}S_{CAS}$ data also show significant variability in certain intervals of the study section and range from +23 to +38‰ (Fig. 4D). In the Five Oaks/Lincolnshire/lower Rockdell, $\delta^{34}S_{CAS}$ values trend from +36 to +26‰, which corresponds to a +1.5‰ $\delta^{13}C_{carb}$ excursion in the Five Oaks/Lincolnshire interval. Another notable perturbation in the $\delta^{34}S_{CAS}$ record is a 4‰ decrease in $\delta^{34}S_{CAS}$ values in the upper Rockdell (~75 m) that predates a negative $\delta^{13}C_{carb}$ shift of 1.2‰. This is followed by two significant positive $\delta^{34}S_{CAS}$ excursions in the overlying Witten Formation (~155 m and ~190 m in stratigraphy). The lower Witten records a +12‰ magnitude excursion in $\delta^{34}S_{CAS}$ that roughly parallels a +8‰ excursion in the $\delta^{13}C_{org}$ record. In the upper Witten, a +12–14‰ excursion in $\delta^{34}S_{CAS}$ parallels positive excursions in both the $\delta^{13}C_{carb}$ and $\delta^{13}C_{org}$ records.

The two $^{87}Sr/^{86}Sr$ data points that were analyzed from the Five Oaks are from samples taken near the base of the section (~0 m) and at approximately 15 m, yielding $^{87}Sr/^{86}Sr$ values of 0.708397 ± 0.000012 and 0.708343 ± 0.000011, respectively (Fig. 3). The $^{87}Sr/^{86}Sr$ value from the Benbolt Formation sample (~120 m) is 0.708292 ± 0.000014.

5. Discussion

We first evaluate factors that may have affected the preservation of primary geochemical signatures (isotopic and elemental abundances), and we then correlate our geochemical records to previously documented $\delta^{13}C_{carb}$ data from other basins that span the globe. Then, first-order trends in $\delta^{34}S$ and $\delta^{13}C$ values are interpreted in terms of possible biogeochemical mechanisms from local depositional/post-depositional environment processes to global changes in the long-term sulfur and carbon cycles. Additionally, we use geochemical box models to test plausible causal mechanisms (e.g., changes in rates of carbonate weathering and organic matter/pyrite burial, different sulfate reservoir sizes, chemocline migration) that may explain observed trends in $\delta^{34}S$ and $\delta^{13}C$. We have highlighted four intervals in the Evans Ferry section to model as they show coupled or decoupled behaviors in the $\delta^{34}S$ and $\delta^{13}C$ records (Five Oaks, Rockdell, lower Witten, and upper Witten; see gray bars in Fig. 4).

5.1. Nature of geochemical signatures

All rocks undergo burial processes that can and, in some cases do, affect their primary geochemical signatures and textural properties. It is of the utmost importance to evaluate whether our observed geochemical records have been significantly affected by diagenetic alteration. We have constructed crossplots of stable isotopic and geochemical data to assess the degree to which these carbonate rocks and paleoenvironmental proxies have been affected by diagenesis (Banner and Hanson, 1990; Oehlert and Swart, 2014). Significant positive covariation

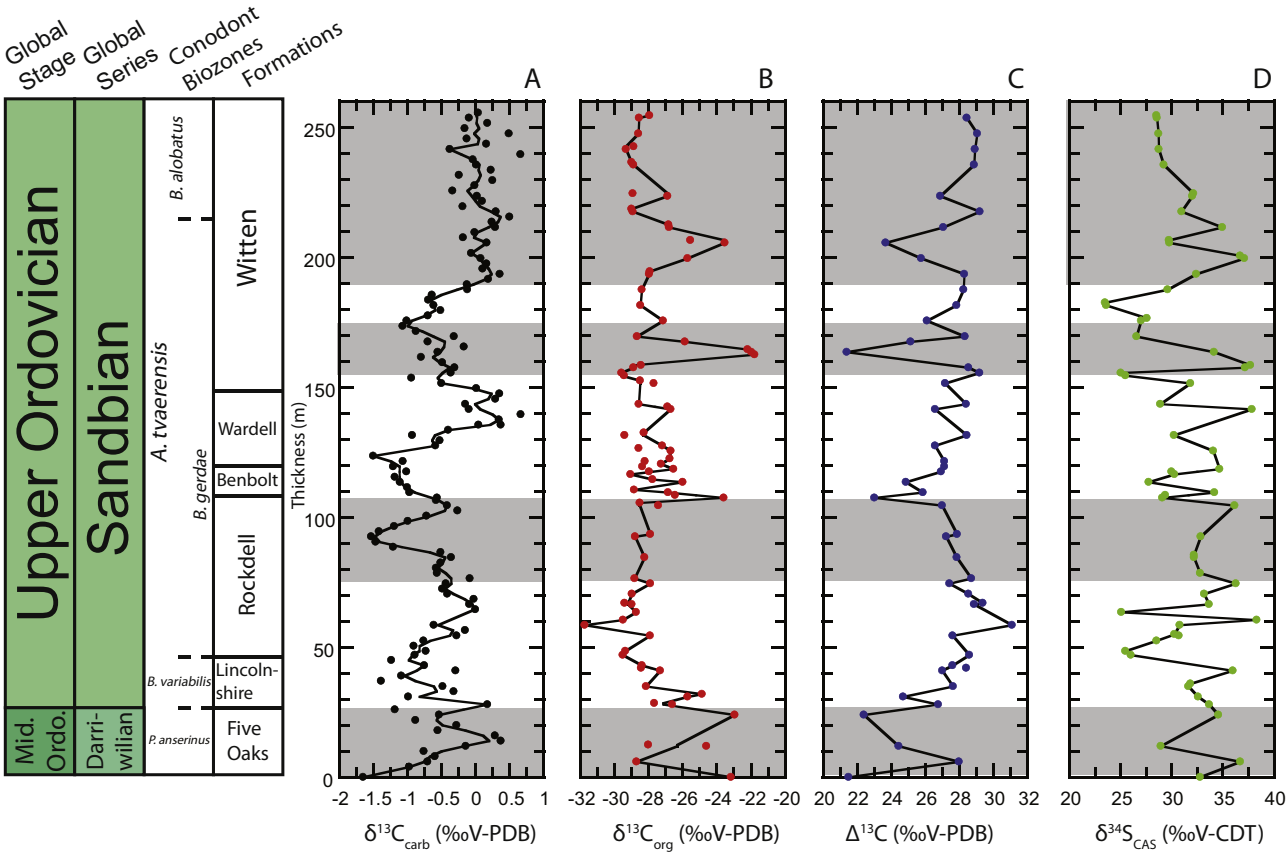

Fig. 4. Stable isotope data from Evans Ferry: A) $\delta^{13}C_{carb}$ values; B) $\delta^{13}C_{org}$ values; C) $\Delta^{13}C$ ($\delta^{13}C_{carb} - \delta^{13}C_{org}$) values; and D) $\delta^{34}S_{CAS}$ values. Note that black lines within each data panel are Lowess best fit lines. Gray boxes indicate intervals of decoupled and coupled stable isotopic data that have been modeled (see Section 5.3.2 through 5.3.4 and Figs. 7–9 for further discussion).

($r > 0.2$) between $\delta^{13}C_{carb}$ and $\delta^{18}O_{carb}$ may indicate possible diagenetic alteration of the stable isotopic values recorded by carbonate rocks (Fike et al., 2006; Metzger and Fike, 2013; Swart and Oehlert, 2018). Crossplots of $\delta^{13}C_{carb}$ and $\delta^{18}O_{carb}$ (Fig. 5B) from the Evans Ferry section ($r = 0.24$, $p < 0.01$, $n = 128$) demonstrate weak correlations for the studied interval. Additionally, $\delta^{13}C_{org}$ may be diagenetically altered through thermal heating and oxidative loss of volatile organic compounds, which might be expected if differential alteration occurs in C_{org}-poor versus C_{org}-rich horizons within a succession (Meyers, 1994). $\delta^{13}C_{org}$ data from the Evans Ferry section show no apparent correlation with wt% TOC (total organic carbon; $r = 0.008$, $p < 0.01$, $n = 128$; Fig. 5A). New studies of shallow-water carbonates suggest that diagenetic changes to $\delta^{13}C_{carb}$ and $\delta^{18}O_{carb}$, as well as other carbonate-bound proxies (e.g., $\delta^{34}S_{CAS}$), can alter their original isotopic compositions (Higgins et al., 2018; Ahm et al., 2018). The Evans Ferry section likely has undergone some degree of diagenetic alteration; however, comparison of the $\delta^{13}C_{carb}$ profile to time-equivalent carbonate datasets from Laurentia and Baltica (Fig. 6) demonstrates that our study section is not altered significantly ($\leq$2‰). Although a minor offset is documented in the Evans Ferry $\delta^{13}C_{carb}$ profile relative to other sequences, it is important to note that the first-order trends are still preserved and corroborated by other sections. It is highly unlikely that all of these carbonate successions from different basins and paleocontinents experienced the same type and degree of diagenesis in a synchronous fashion to explain the excellent overall agreement in $\delta^{13}C_{carb}$ trends (Fig. 6). Therefore, we interpret these data as secular trends in Ordovician seawater rather than signatures of diagenesis, which is largely a local process.

It is also important to address diagenetic concerns regarding our CAS extractions and their corresponding $\delta^{34}S$ values. Studies by Gill et al. (2008) and Sim et al. (2015) have shown that, while meteoric diagenesis can significantly lower CAS concentrations within marine carbonates, it has little to no effect on $\delta^{34}S_{CAS}$ values. Crossplots of $\delta^{18}O_{carb}$ vs. $\delta^{34}S_{CAS}$, $\delta^{18}O_{carb}$ vs. [CAS], and $\delta^{34}S_{CAS}$ vs. [CAS] (Fig. 5C, D, E) show no significant correlation ($r = 0.00009$, $p = 0.70$, $n = 43$; $r = 0.0001$, $p = 0.35$, $n = 43$; $r = 0.0025$, $p < 0.01$, $n = 43$, respectively), suggesting that the $\delta^{34}S_{CAS}$ values have not been significantly affected by diagenesis. Another potential concern to address is incorporation of contaminant sulfate into the CAS fraction through oxidation of sedimentary pyrite during diagenesis or chemical extraction, as this can artificially lower $\delta^{34}S_{CAS}$ values (Marenco et al., 2008). Although extractions of sedimentary pyrite and $\delta^{34}S_{pyr}$ analysis were not performed for this study, extensive petrographic examination of carbonate strata from our study section was performed and yielded little (< 1 wt%) to no pyrite in any of the sampled horizons, and stratigraphic intervals that had visible pyrite or iron-oxide staining were specifically avoided during sample collection. In addition, rinsing and leaching steps between carbonate digestion and barite extraction were utilized to ensure that oxidation of pyrite and secondary atmospheric sulfate did not contaminate the extractable CAS fractions (Wotte et al., 2012; Peng et al., 2014). Another concern for the primary nature of $\delta^{34}S_{CAS}$ values is dolomitization, especially within the Wardell Formation at Evans Ferry, as a significant portion of this formation is mixed dolostone and limestone. Marenco et al. (2008) found that $\delta^{34}S_{CAS}$ values from dolostones are significantly lighter than those of correlative limestones. Other studies have shown, however, that secondary dolomitization has little effect on $\delta^{34}S_{CAS}$ values and again only affects [CAS] (Kah et al., 2004; Hurtgen et al., 2006; Shen et al., 2008). The validity of bulk $\delta^{34}S_{CAS}$ signatures has recently been called in to question due to significant variation in $\delta^{34}S_{CAS}$ values between different

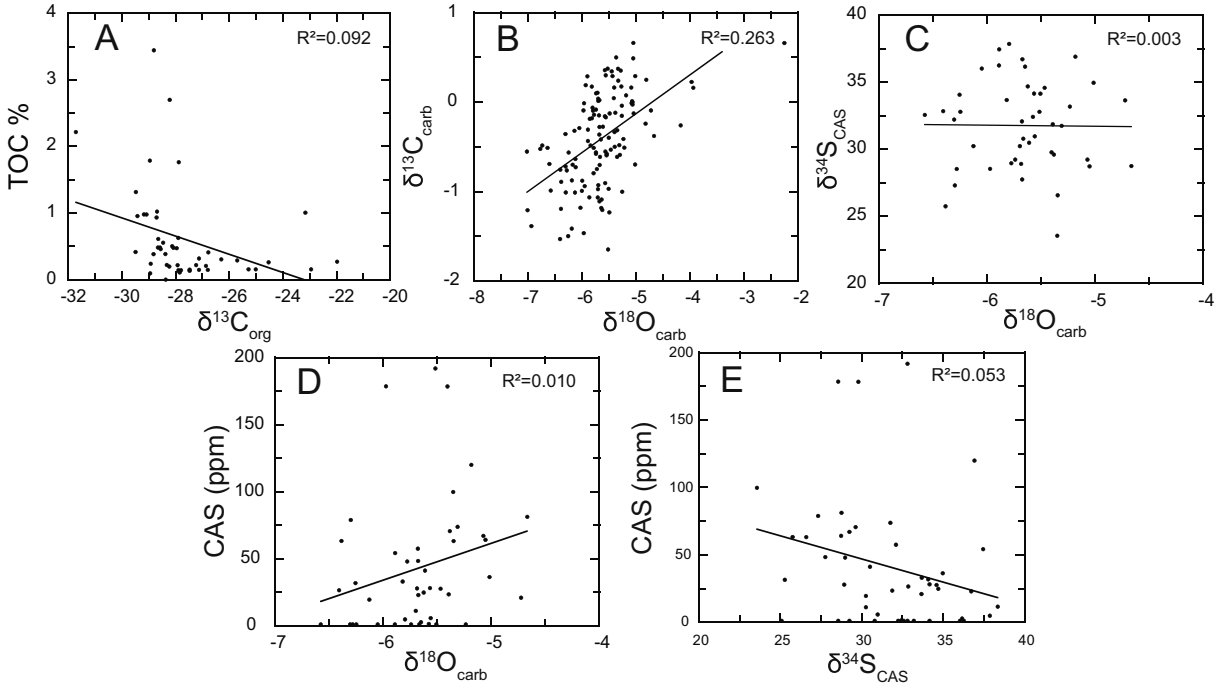

Fig. 5. Cross-plots for diagenetic evaluation (see Section 5.2 for discussion). A) TOC (wt%) vs $\delta^{13}C_{org}$; $n = 128$. B) $\delta^{18}O_{carb}$ vs $\delta^{13}C_{carb}$; $n = 128$C) $\delta^{34}S_{CAS}$ vs $\delta^{18}O_{carb}$; $n = 43$. D) [CAS] (ppm) vs $\delta^{18}O_{carb}$; $n = 43$. E) [CAS] (ppm) vs $\delta^{34}S_{CAS;}$ $n = 43$.

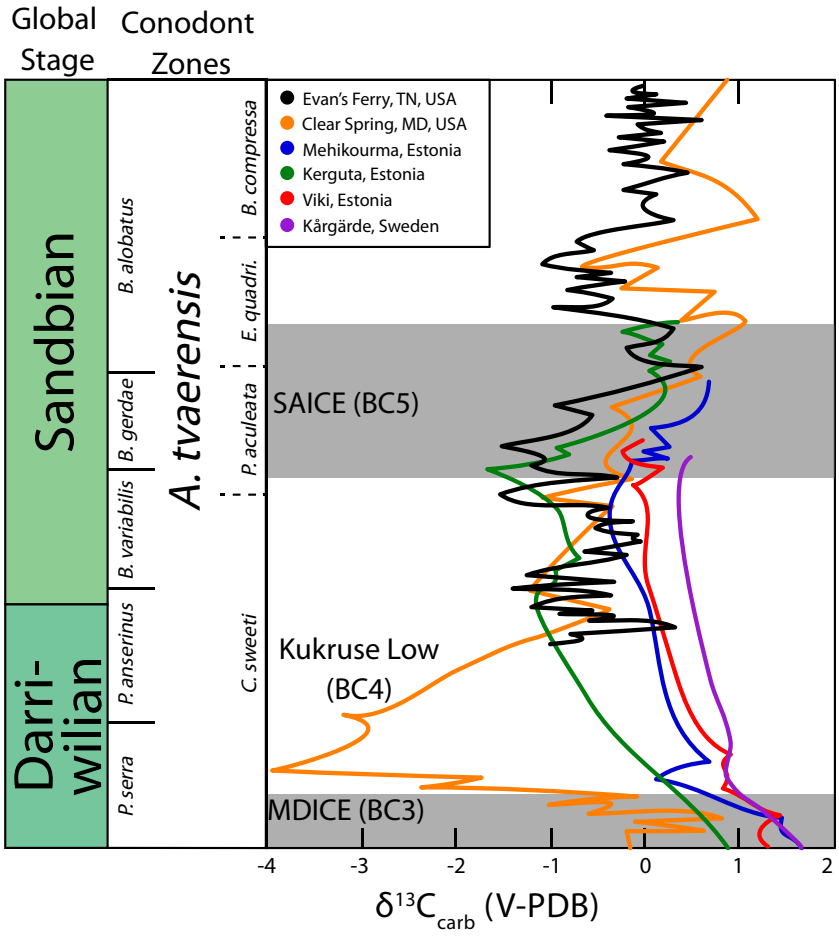

Fig. 6. Correlation of $\delta^{13}C_{carb}$ trends from eastern North American and Baltoscandian sections through the upper Darriwilian–Sandbian Stages. Clear Spring, MD data are from Saltzman and Edwards (2017), and the Baltoscandian data are from Ainsaar et al. (2010).

carbonate components in the same sample (Present et al., 2015). Present et al. (2015) suggested that brachiopods are the most reliable carbonate component for CAS analyses; however, their findings were based upon a single section from the Hirnantian Stage of the Ordovician, and therefore more studies are needed to determine if their findings are applicable to all stratigraphic records. Regardless, brachiopod-rich horizons do not occur with enough frequency or regularity at Evans Ferry to make this a viable option for high-resolution chemostratigraphic studies. Similar to carbon isotopes, $\delta^{34}S_{CAS}$ values from the Evans Ferry section may reflect some degree of diagenesis; however, there is no evidence that the overall trends presented here do not reflect global trends of Ordovician seawater sulfate. If $\delta^{34}S_{CAS}$ values were significantly altered through diagenetic processes and largely not reflective of secular trends of seawater sulfate, then we would not expect to observe broad-scale trends in the data that continue through changes in carbonate facies and across formation boundaries. Rather, we would expect that $\delta^{34}S_{CAS}$ values would be highly variable between samples. Ultimately, to confirm that our $\delta^{34}S_{CAS}$ records are indeed representative of global seawater trends, high-resolution $\delta^{34}S_{CAS}$ datasets will be needed for time-equivalent sections from other basins and paleocontinents.

5.2. Correlation with other Darriwilian–Sandbian $\delta^{13}C$, $\delta^{34}S$, and sequence stratigraphic records

This study utilizes conodont biostratigraphy (Carnes, 1975; Bergström and Carnes, 1985) and new conodont-apatite $^{87}Sr/^{86}Sr$ analyses within the Evans Ferry section to determine a robust age model for this Appalachian Basin succession. The Evans Ferry section primarily contains non-diagnostic North American Midcontinent conodonts that range from the late Darriwilian through the Sandbian. Our new conodont $^{87}Sr/^{86}Sr$ values from the Five Oaks (0.70839 at the base and 0.70834 in the middle) and Benbolt (0.70829) formations provide robust age constraints on the lower and middle portions of the Evans Ferry succession despite non-diagnostic conodont faunas (i.e., Bergström and Carnes, 1985). When these new conodont $^{87}Sr/^{86}Sr$ values are integrated with a recent conodont-apatite based $^{87}Sr/^{86}Sr$ seawater curve for the Ordovician (Fig. 3; Saltzman et al., 2014), this Sr isotope stratigraphy (SIS) places additional temporal constraints on the lower and middle portions of the Evans Ferry succession. By comparing the Evans Ferry data with the Saltzman et al. (2014) conodont-based $^{87}Sr/^{86}Sr$ profile, we obtain a very highly resolved (at ~1–2 Myr) age model for the upper Darriwilian–Sandbian interval (Fig. 3). In contrast, the conodont biostratigraphic data alone would yield a much coarser (> 5 Myr) resolution due to the non-diagnostic taxa present (Carnes, 1975; Saltzman et al., 2014).

The Evans Ferry section (an expanded uppermost Darriwilian and Sandbian sequence) allows for identification high-resolution chemostratigraphic trends that may be difficult to discern in other sections of equivalent age (e.g., Midcontinent USA, Baltica; Ainsaar et al., 2010; Bergström et al., 2010). Studies from Baltica and other basins in North America have observed broad-scale trends such as the Mid-Darriwilian Carbon Isotope Excursion (MDICE) and Sandbian Isotope Shift (also referred to as UDIS or SAICE; Bergström et al., 2016; Saltzman and Edwards, 2017); however, our higher resolution study shows more detailed $\delta^{13}C$ and $\delta^{34}S_{CAS}$ trends than those of other relatively condensed or coarsely sampled Sandbian successions (e.g. Ainsaar et al., 2010; Edwards and Saltzman, 2015; Young et al., 2016).

The ~+2‰ positive shift in $\delta^{13}C_{carb}$ values within the Five Oaks Fm. (occurring at ~15 m, within the *P. anserinus* Biozone) is of similar magnitude and chronostratigraphic position (i.e., almost identical SIS) as a ~+2‰ positive shift in $\delta^{13}C_{carb}$ values within the middle New Market Formation at Clear Spring, Maryland (e.g., Saltzman and Edwards, 2017). In addition to this positive shift, there is a 1‰ negative excursion found in the upper New Market Formation (occurring within the *B. gerdae* Biozone) at Clear Spring that is correlative to the 1.5‰ negative excursion documented within the upper Rockdell Fm. at Evans Ferry (~90 m; Fig. 6). Last, our $\delta^{13}C_{carb}$ dataset within the Witten Formation, as well as most other datasets from Baltica and Laurentia, shows that the SAICE occurs within the same upper *B. gerdae* through lower *B. alobatus* conodont biozones. All of these correlative $\delta^{13}C_{carb}$ shifts indicate that, while this basin may have experienced some local restriction during relative sea-level lowstands (Fig. 3), first-order trends observed in $\delta^{13}C_{carb}$ values in time-equivalent strata from other basins across Laurentia and Baltica are also recorded at Evans Ferry, Tennessee. Similarly, $\delta^{34}S_{CAS}$ records in the Bromide Formation in the Arbuckle Mountains, Oklahoma, record a ~+10‰ excursion (Young et al., 2016), which is correlative to the large-magnitude excursion documented in $\delta^{34}S_{CAS}$ values from the Witten (~190 m).

Sequence stratigraphic analysis of the Evans Ferry section reveals three complete sea-level cycles (Fig. 3) that are ~1–3 Myr in duration (e.g., third-order cycles; Vail et al., 1977). A recent study of the time-equivalent Tulip Creek and Bromide formations in the Arkhoma Basin of Oklahoma also documented three third-order sequences (Carlucci et al., 2014). The broad similarities in local sea-level reconstructions and changes in the overall patterns in carbonate facies observed in both the Evans Ferry and the Arbuckle Mountains successions likely indicate that a eustatic sea-level signature is present in this part of the Appalachian Basin, despite the Taconic Orogeny influencing local accommodation space. The local sea-level curve from Evans Ferry is also broadly consistent with previous sequence stratigraphic studies that are considered to represent Ordovician eustasy (Nielsen, 2004; Haq and Schutter, 2008).

5.3. Mechanisms and models for $\delta^{13}C$ and $\delta^{34}S$ trends

There are three primary mechanisms that control seawater $\delta^{13}C_{DIC}$, and therefore $\delta^{13}C_{carb}$, values: the burial fraction of organic carbon (F_{org}), the weathering flux (F_w), and the photosynthetic fractionation factor between $\delta^{13}C_{DIC}$ and the resulting organic matter ($\varepsilon_p \approx \Delta^{13}C$) (e.g., Kump and Arthur, 1999; Kump et al., 1999). The removal of isotopically light carbon through the burial of organic matter leaves the oceanic $\delta^{13}C_{DIC}$ composition isotopically heavy and can result in positive carbon isotope excursions. If organic matter is remineralized before burial, however, then it can release ^{12}C-enriched carbon back to the water column and potentially cause local carbon isotope excursions. The oxidative weathering of carbonates and organic-rich sedimentary rocks (F_w) is the largest flux of carbon into the oceans. With a distinctive isotope signature of modern rivers ($\delta^{13}C_{riv} = -4‰$), significant increases in this flux can shift oceanic $\delta^{13}C_{DIC}$ values toward riverine endmember values (Kump and Garrels, 1986; Kump and Arthur, 1999; Kurtz et al., 2003). Changes in the ratio of weathered lithologies (i.e., a shift to more carbonate and less organic-rich rocks with the onset of eustatic regression) can alter $\delta^{13}C_{riv}$ and ultimately $\delta^{13}C_{carb}$ values (e.g., Kump et al., 1999). Lastly, a change in the fractionation factor (ε_p) between DIC and organic matter can affect $\delta^{13}C$ records. Previous studies have shown that $\Delta^{13}C$ values can be affected by factors such as phytoplankton growth rates and cell shape, pCO_2, and pO_2 (Bidigare et al., 1997; Popp et al., 1998; Berner et al., 2000).

Similar to $\delta^{13}C_{carb}$, three primary factors may also cause changes in $\delta^{34}S_{CAS}$ values: the burial fraction of sedimentary pyrite under euxinic conditions (F_{pyr}), the riverine input of weathered sulfate and sulfide minerals (F_W), and changes in fractionation between the reactant (sulfate) and product (H_2S) during MSR ($\varepsilon_{SR} \approx \Delta^{34}S$). Pyrite burial rates are modulated by factors such as water column redox state and the availability of sulfate, labile organic matter, and iron in the depositional environment (Berner, 1985). Within a well-oxygenated water column, MSR can be limited as the produced H_2S will be oxidized back to sulfate, which reintroduces isotopically light sulfur back into the water column (Canfield, 2001). In addition, if the burial site of organic matter changes, this may also influence MSR rates by limiting the fuel source of this metabolic pathway, and allowing for the decoupling of the C and S

isotopic trends (Leavitt et al., 2013). Enhanced burial of organic matter, a key component to MSR, can be reflected in $\delta^{13}C_{carb}$ records, and may covary with enhanced burial of pyrite, which can be reflected in $\delta^{34}S_{CAS}$ records. Reduced iron may also be a limiting factor in pyrite formation and subsequent burial. If marine anoxia is not prevalent, iron oxides will not be reduced to Fe^{2+}, which can inhibit the formation of pyrite in both the water column and sediments (Canfield et al., 1992). The oxidative weathering of sulfur-bearing minerals on land is the largest input of sulfur to the oceans (modern $\delta^{34}S_{riv} = +4.8‰$), and it also can influence the isotopic composition of seawater sulfate (Burke et al., 2018). Lastly, changes in fractionation between sulfate and sedimentary pyrite, as measured by $\Delta^{34}S$, may affect stratigraphic trends in sulfur isotopes. $\Delta^{34}S$ is affected by a variety of factors including sulfate concentrations, sulfur disproportionation, cell specific MSR rates, and fluid exchange in sediment porewaters (Amend et al., 2004; Kah et al., 2004; Sim et al., 2011a, 2011b; Leavitt et al., 2013).

To better understand the possible mechanisms driving Middle–Late Ordovician carbon and sulfur excursions at Evans Ferry, we created forward geochemical box models. Our models use parameters similar to Kurtz et al. (2003) and Gill et al. (2011) (see data repository for initial modeling parameters). Here, we discuss modeling scenarios for the four intervals of interest within the Five Oaks, Rockdell, and Witten formations. We also present new modeling scenarios for the Rockdell, lower Witten, and upper Witten intervals at Evans Ferry. These geochemical box models explore both individual mechanisms and combination of mechanisms that could produce our recorded isotopic trends. Our forward box models reproduce the $\delta^{13}C$ and $\delta^{34}S_{CAS}$ trends with transient changes to the carbon and sulfur cycles lasting ~0.5 million years, and we examine each of the scenarios in the following sections.

5.3.1. Five Oaks interval

The antithetical $\delta^{13}C_{carb}$ and $\delta^{34}S_{CAS}$ trends recorded during a sea-level lowstand in the Five Oaks interval are correlative with carbon and sulfur trends in the New Market and Chambersburg formations at Clear Spring, Maryland (Young et al., 2016). Young et al. (2016) determined that a reduction in pyrite burial coupled to a reduction of organic matter remineralization is the most parsimonious explanation for the decoupled $\delta^{13}C_{carb}$ and $\delta^{34}S_{CAS}$ trends, as changes in the weathering fluxes alone cannot reproduce these patterns. Furthermore, at the Evans Ferry section, these inverse $\delta^{13}C_{carb}$ and $\delta^{34}S_{CAS}$ trends are documented in strata deposited above the Knox unconformity and in equivalent strata at Clear Spring (i.e., upper New Market Formation), where a similar return to open-marine conditions is documented (Saltzman and Edwards, 2017). The overall similar sedimentological, faunal, and $\delta^{13}C_{carb}$ and $\delta^{34}S_{CAS}$ trends (antithetical relationship) between the Evans Ferry and Clear Spring sections support the previous interpretations (Young et al., 2016). Therefore, we have not modeled the $\delta^{13}C_{carb}$ and $\delta^{34}S_{CAS}$ trends from this interval of the Evans Ferry section.

5.3.2. Rockdell interval

The upper Rockdell Formation records a 2‰ drop in $\delta^{13}C_{carb}$ values (~90 m) that begins just after a 4‰ decline in $\delta^{34}S_{CAS}$ values (Fig. 4), and this may reflect the difference in response times of the carbon (DIC) and sulfate reservoirs in Ordovician oceans. The Ordovician marine sulfate reservoir was likely significantly smaller than modern levels (Algeo et al., 2015), which makes the sulfur cycle more responsive to perturbations (Gill et al., 2011; Thompson et al., 2012; Young et al., 2016). The carbon and sulfur isotope trends in the Rockdell interval can be attributed to changes in the weathering or riverine input (F_w), and these changes may have been driven by uplift and weathering in the newly formed Taconic highlands (e.g., Young et al., 2009; Swanson-Hysell and Macdonald, 2017). Our forward box model simulations show that by increasing F_w by 75% it is possible to generate the 2‰ decrease in $\delta^{13}C_{carb}$ values and the ~4‰ decline in $\delta^{34}S_{CAS}$ values (Fig. 7A). The Rockdell Fm., however, is interpreted to have been deposited in a highstand systems tract (Pope and Read, 1998), which is consistent with our sequence stratigraphic analysis (Fig. 3 and Section 5.2). Therefore, an increase in F_w alone may not have been the primary driver of these negative shifts in $\delta^{13}C_{carb}$ and $\delta^{34}S_{CAS}$ for the Rockdell interval.

These decreasing isotope trends within the Rockdell interval can instead be linked to reductions in pyrite and organic matter burial via increases in marine water-column oxygenation. A decrease of organic

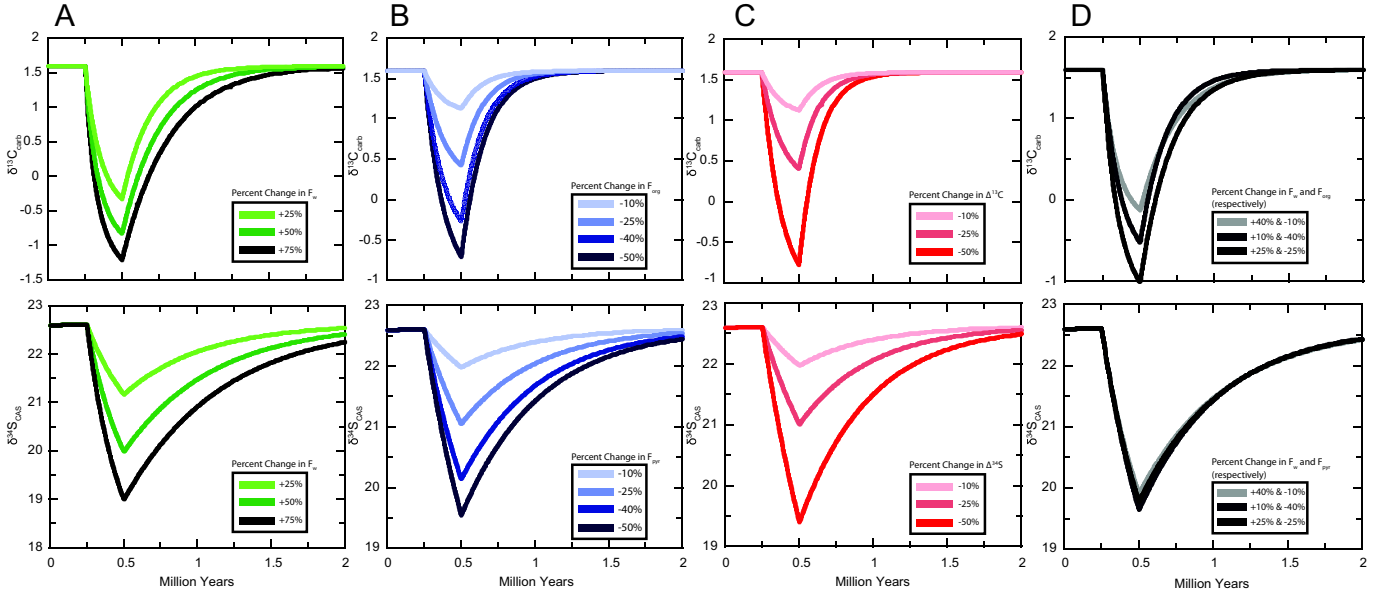

Fig. 7. Results from geochemical box model simulations for the upper Rockdell interval. A) The resulting marine carbonate ($\delta^{13}C_{carb}$) and sulfate ($\delta^{34}S_{CAS}$) trends due to varying changes in riverine inputs (F_w). B) The resulting marine carbonate ($\delta^{13}C_{carb}$) and sulfate ($\delta^{34}S_{CAS}$) trends due to varying changes in the burial fluxes (F_{org} and F_{pyr}, respectively). C) The resulting marine carbonate ($\delta^{13}C_{carb}$) and sulfate ($\delta^{34}S_{CAS}$) trends due to varying changes the fractionation factor between reduced and oxidized species ($\Delta^{13}C$ and $\Delta^{34}S$, respectively). D) The resulting marine carbonate ($\delta^{13}C_{carb}$) and sulfate ($\delta^{34}S_{CAS}$) trends due to varying changes in both riverine inputs and burial fluxes. Legends indicate magnitude of deviation from steady state for each sensitivity test. All top panels compare $\delta^{13}C_{carb}$ through the simulated time, while all bottom panels compare $\delta^{34}S_{CAS}$ values through the same simulated time. In these simulations initial $[SO_4^{2-}]$ was set to 1.5 mM.

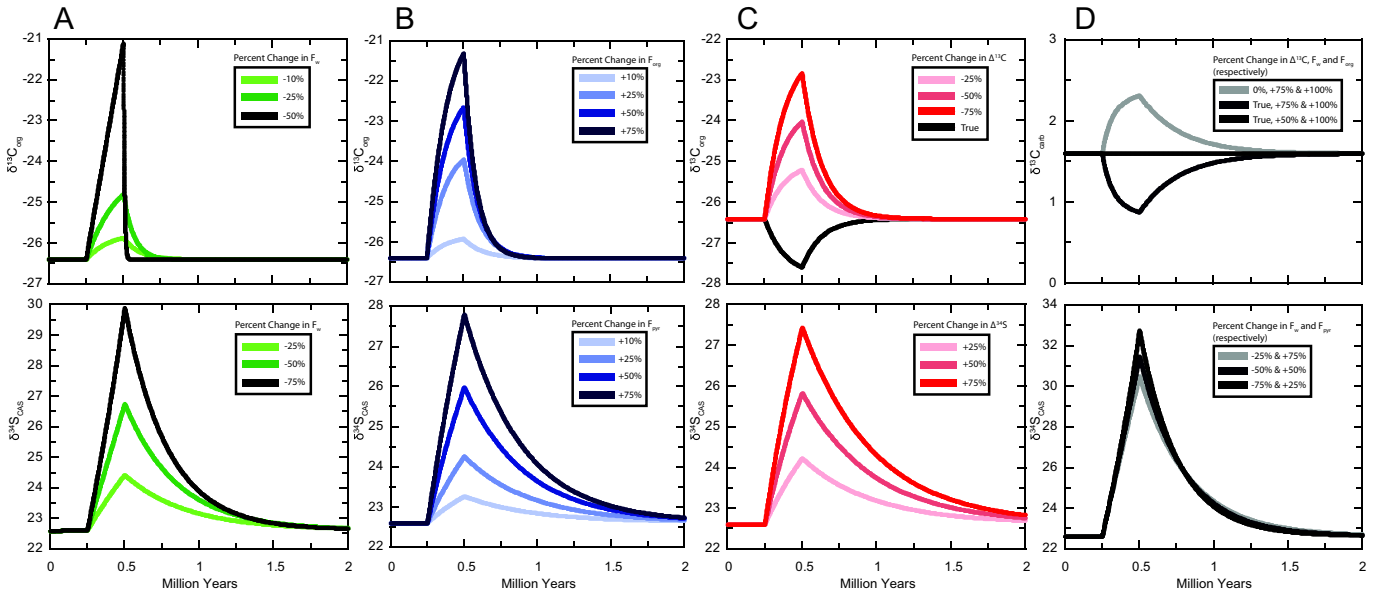

Fig. 8. Results from geochemical box model simulations for the lower Witten interval. A) The resulting bulk organic matter ($\delta^{13}C_{org}$) and sulfate ($\delta^{34}S_{CAS}$) trends due to varying changes in riverine inputs (F_w). B) The resulting bulk organic matter ($\delta^{13}C_{org}$) and sulfate ($\delta^{34}S_{CAS}$) trends due to varying changes in the burial fluxes (F_{org} and F_{pyr}, respectively). C) The resulting marine bulk organic matter ($\delta^{13}C_{org}$) and sulfate ($\delta^{34}S_{CAS}$) trends due to varying changes the fractionation factor between reduced and oxidized species ($\Delta^{13}C$ and $\Delta^{34}S$, respectively). The black "True" line indicates the maximum $\Delta^{13}C$ values found through the corresponding interval from the Evans Ferry section and is the same through panel D. D) The resulting marine carbonate ($\delta^{13}C_{carb}$) and sulfate ($\delta^{34}S_{CAS}$) trends due to varying changes in the fractionation factor (for carbon only), riverine inputs, and burial fluxes. Legends indicate magnitude of deviations from steady state for each sensitivity test. In these simulations initial [SO_4^{2-}] was set to 1.5 mM.

matter flux to the seafloor can limit the amount of MSR activity, as this metabolic pathway is directly linked to the availability of labile electron donors, resulting in a decrease in pyrite formation and thus a reduction in burial (Leavitt et al., 2013). Our model (Fig. 7B) shows that a 50% decrease in the burial fluxes of organic matter and pyrite (F_{org} and F_{pyr} respectively) can produce similar trends. This reduction in F_{org} and F_{pyr} may represent a decrease in the preservation potential of organic matter and pyrite due to increases in remineralization and oxidation rates. These reductions in F_{org} and F_{pyr} can be linked to oceanic ventilation (Jones and Fike, 2013; Young et al., 2016), which may have also driven the chemocline deeper within the sediments. This process may account for the concurrent decrease in $\Delta^{34}S$ values (see discussion below).

Another modeling scenario that can produce the observed shifts in the upper Rockdell is a change in the photosynthetic fractionation factor between DIC and organic matter (ε_p), as well as between sulfate and sulfide during MSR (ε_{SR}). A change in ε_p is not necessarily supported, however, as our $\Delta^{13}C$ values only show a small decrease from 28‰ to 26‰ through this interval. Furthermore, by changing this variable alone, it is not possible to replicate the 2‰ decrease in $\delta^{13}C_{carb}$. Since variations in $\Delta^{13}C$ documented within the rock record are unable solely to drive the observed $\delta^{13}C_{carb}$ trends, we can eliminate this variable as the sole mechanism controlling this negative excursion. Our modeling efforts, however, did include changing the fractionation factor between seawater sulfate and pyrite. We found that a transient lowering of $\Delta^{34}S$ alone could produce the decline in $\delta^{34}S_{CAS}$ of the Rockdell interval; a sensitivity test shows that a 50% decline in $\Delta^{34}S$ over 0.5 million years is sufficient to reproduce this $\delta^{34}S_{CAS}$ trend (Fig. 7C). Changes in cell-specific rates of MSR have been invoked for decreases in $\Delta^{34}S$ during the Hirnantian that were coincident with a positive $\delta^{13}C_{carb}$ excursion and glaciation, under which increased rates of MSR were fueled by waning aerobic decomposition of organic matter (Jones and Fike, 2013). There are no known glacial deposits of Darriwilian-Sandbian age (e.g., Frakes et al., 1992), but recent $\delta^{18}O$ data suggest cooling intervals as far back as the Darriwilian (Rasmussen et al., 2016). Conodont-phosphate $\delta^{18}O$ data (sea-surface temperature proxy) show stable temperatures (Trotter et al., 2008), which suggests climate-induced biological factors are unlikely to explain scenarios that invoke decreases in $\Delta^{34}S$ or $\Delta^{13}C$.

It is important to note that concurrent changes in the aforementioned mechanisms can produce the observed isotopic trends within the Rockdell interval (Fig. 7D). Changes in both weathering and organic matter burial may have occurred simultaneously, as suggested by previous geochemical models and geologic evidence (e.g., Young et al., 2009; Edwards et al., 2017). We chose not include shifts in $\Delta^{13}C$ or $\Delta^{34}S$ in our flux combination model simulations due to lack of geologic or geochemical evidence for significant changes in fractionation factors during the Sandbian. In our combined-flux modeling efforts, tandem changes in weathering and burial fluxes in varying degrees can reproduce observed $\delta^{13}C_{carb}$ and $\delta^{34}S_{CAS}$ records trends in the Rockdell interval (Fig. 7D).

5.3.3. Lower Witten interval

Another interval of decoupled $\delta^{13}C$ and $\delta^{34}S$ trends is documented within the lower Witten Fm. Here, $\delta^{13}C_{carb}$ remains in a relatively steady state (values at $-0.5‰ \pm 0.5$) while $\delta^{34}S_{CAS}$ signatures increase by 12‰. It is also important to note this change in $\delta^{34}S_{CAS}$ begins just prior (~155 m) to a large 8‰ increase in $\delta^{13}C_{org}$ (~160 m). The box model simulations of the lower Witten interval show that a decrease in the F_w of carbon (50%) and sulfur (75%) can reproduce the $\delta^{13}C_{org}$ and $\delta^{34}S_{CAS}$ stratigraphic trends (Fig. 8A). It is not possible, however, to reproduce the invariant $\delta^{13}C_{carb}$ trends during this same interval solely by changing F_w. Decreasing weathering fluxes are not consistent with a Sandbian sea-level rise and the ongoing Taconic Orogeny, which led to increased accommodation space in the foreland basin (Ettensohn and Lierman, 2012). Furthermore, sequence stratigraphic analysis through this interval shows an overall restricted set of carbonate facies that represents a relative sea-level lowstand. The lithofacies in the lower Witten interval suggest a transition from an open-marine carbonate ramp to a restricted lagoonal environment, which is indicated by the appearance of oncoidal packstones, laminated microbialites, and abundant desiccation cracks within this interval. As

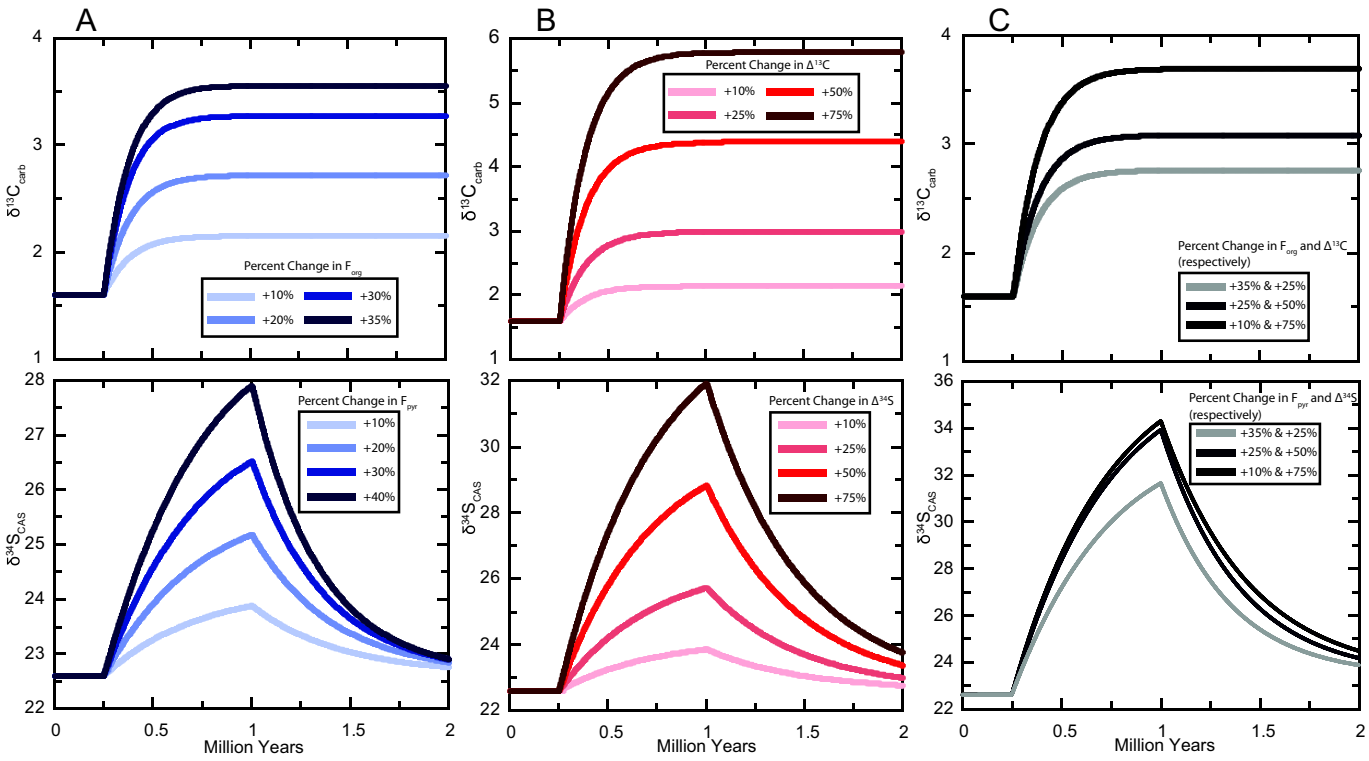

Fig. 9. Results from geochemical box model simulations for the upper Witten interval. A) The resulting marine carbonate ($\delta^{13}C_{carb}$) and sulfate ($\delta^{34}S_{CAS}$) trends due to varying changes in the burial fluxes (F_{org} and F_{pyr}, respectively). B) The resulting marine carbonate ($\delta^{13}C_{carb}$) and sulfate ($\delta^{34}S_{CAS}$) trends due to varying changes the fractionation factor between reduced and oxidized species ($\Delta^{13}C$ and $\Delta^{34}S$, respectively). C) The resulting marine carbonate ($\delta^{13}C_{carb}$) and sulfate ($\delta^{34}S_{CAS}$) trends due to varying changes in both riverine inputs and burial fluxes. Legends indicate the magnitude of deviations from steady state for each sensitivity test. In these simulations initial [SO_4^{2-}] was set to 1.5 mM.

progressive restriction occurred within the basin, local conditions (e.g., increases in pyrite and organic matter burial) became the predominant factors controlling local $\delta^{13}C$ and $\delta^{34}S$ seawater values (Panchuk et al., 2005; Gomes and Hurtgen, 2015).

Our modeling results show that a 75% increase in F_{org} and a 75% increase in F_{pyr} can reproduce the observed changes in $\delta^{13}C_{org}$ and $\delta^{34}S_{CAS}$ (Fig. 8B). The $\delta^{13}C_{carb}$ and $\delta^{13}C_{org}$ records should mirror one another, however, as organic matter isotopic signatures are influenced by the marine DIC isotopic composition, as well as photosynthetic isotopic fractionation (~ −28‰) (Kump and Arthur, 1999). Our models show that changing $\Delta^{13}C$ alone by the amount recorded in the lower Witten ($\Delta^{13}C = -21$‰) generates an inverse trend in $\delta^{13}C_{org}$, which is inconsistent with the observed +8‰ excursion (Fig. 8C).

It is important to note that it is not possible to reproduce the observed $\delta^{13}C$ and $\delta^{34}S$ trends in the lower Witten by changing just a single model parameter. In order to reproduce the $\delta^{13}C$ and $\delta^{34}S$ trends, three model parameters were changed simultaneously (Fig. 8D): F_{pyr} and F_{org} were increased by 50–75% and F_w by 50%, allowing calculated $\Delta^{13}C$ to match observed $\Delta^{13}C$ values (−21‰). All three model parameters must be varied simultaneously in order to create an acceptable modeling solution for the observed stable isotopic signatures recorded within the lower Witten Formation. When the geochemical modeling scenarios for the isotopic records documented within this interval are combined with the lithologic evidence for basin restriction and relative sea-level fall, it seems that these $\delta^{13}C_{org}$ and $\delta^{34}S_{CAS}$ records are likely representative of increasingly closed-system behavior associated with local biogeochemical cycling (e.g., within sediment porewaters, sediment-water interface) rather than of secular changes in global seawater.

5.3.4. Upper Witten interval

The final scenario that was modeled in this study is the coupled carbon and sulfur isotopic behavior seen in the upper part of the Witten Formation (~180 to 240 m). In this interval, $\delta^{13}C_{carb}$ values increase by +1.5‰, $\delta^{13}C_{org}$ values increase by +8‰, and $\delta^{34}S_{CAS}$ values show a +10‰ excursion (Fig. 4). It was not possible to recreate the observed $\delta^{13}C$ and $\delta^{34}S$ trends by changing only the F_w of carbon and sulfur in any box model simulations. By adjusting the F_{org} and F_{pyr} parameters, however, we were able to recreate the observed $\delta^{13}C$ and $\delta^{34}S$ trends, specifically by increasing F_{org} by 20% and F_{pyr} by 35% (Fig. 9A). We also found acceptable modeling solutions by increasing $\Delta^{13}C$ and $\Delta^{34}S$ by 25% and 75%, respectively (Fig. 9B). The $\Delta^{13}C$ values, however, had to be allowed to rise beyond their observed range in the Evans Ferry section in order to reproduce the stratigraphic trends in $\delta^{13}C$ and $\delta^{34}S$. Consequently, a more plausible modeling solution for the upper Witten interval involves a combination of modest increases in F_{org} and F_{pyr} along with increases in $\Delta^{13}C$ and $\Delta^{34}S$ (Fig. 9C).

6. Conclusions

In this study, we have documented multiple low-magnitude $\delta^{13}C_{carb}$ fluctuations (~1.5–2‰) that can be correlated to other basins in Laurentia and Baltica, and several of these $\delta^{13}C_{carb}$ shifts have coincident $\delta^{34}S_{CAS}$ perturbations (4–12‰). The results from this study have several implications for future integrated chemostratigraphic and geochemical box modeling studies. The modeling efforts show complex and seemingly disparate $\delta^{13}C$ and $\delta^{34}S$ chemostratigraphic trends can only be recreated by changing a combination of several parameters. These intricate modeling solutions support the notion that local processes (e.g., increased closed-system behavior, sediment reworking) become the predominant influence on $\delta^{13}C$ and $\delta^{34}S$ chemostratigraphic trends during intervals when geologic evidence suggests environmental restriction and non-open marine conditions.

Future multiproxy work in Darriwilian–Sandbian strata will help to discern whether paleoredox conditions are the predominant factor driving the $\delta^{13}C_{carb}$ and $\delta^{34}S_{CAS}$ records reported here. We interpret the intervals of antithetical $\delta^{13}C_{carb}$ and $\delta^{34}S_{CAS}$ trends to be the product of both a reduction of global pyrite burial rates and increasing marine sulfate concentrations during intervals of more oxic marine conditions, while coupled positive shifts in $\delta^{13}C_{carb}$ and $\delta^{34}S_{CAS}$ trends are suggested to reflect a return to more reducing conditions in the global oceans. Also associated with these alternating marine redox conditions, sea level was approaching its highest levels in the Ordovician (and much of the Paleozoic) with epeiric seaways spanning many paleocontinents during this time. The cooling that occurred in the Middle-Late Ordovician may have led to more vigorous thermohaline circulation as well as a greater capacity for the ocean to hold dissolved atmospheric CO_2 and O_2. Increasing the amount of dissolved O_2 in the Ordovician oceans would have created new niche spaces where marine organisms could diversify. Prolonged cycling between oxic and more reducing global marine redox conditions may have also been a key environmental process linked to observed changes in the rates and severity of extinctions in graptolites and other marine taxa throughout the Late Ordovician, which suggests a close relationship between environmental conditions and biodiversity at that time.

Acknowledgments

We thank Jeremy Owens and Angela Knapp for their insightful discussions throughout the writing process. Additionally, we thank Editor Tom Algeo, Cole Edwards, and an anonymous reviewer for their very detailed comments that helped to significantly strengthen our manuscript. We would also like to thank the Young Lab Group at FSU for their support and assistance in sample collection and sample preparation: Andrew Kleinberg, Emily Benayoun, Hilary Davis and Lance Newman. Additionally, we would like to thank Burt Wolff at the National High Magnetic Field Laboratory (NHMFL) for his help with the carbon and oxygen isotope analysis and Benjamin Underwood at Indiana University for his help with the sulfur isotope analysis. This work was performed at the National High Magnetic Field Laboratory, which is supported by the National Science Foundation Cooperative Agreement No. DMR-1644779 and the State of Florida.

Appendix A. Supplementary data

Supplementary data to this article can be found online at https://doi.org/10.1016/j.palaeo.2019.01.032.

References

Ahm, A.S.C., Bjerrum, C.J., Blättler, C.L., Swart, P.K., Higgins, J.A., 2018. Quantifying early marine diagenesis in shallow-water carbonate sediments. Geochim. Cosmochim. Acta 236, 140–159. https://doi.org/10.1016/j.gca.2018.02.042.

Ainsaar, L., Kaljo, D., Martma, T., Meidla, T., Männik, P., Nõlvak, J., Tinn, O., 2010. Middle and Upper Ordovician carbon isotope chemostratigraphy in Baltoscandia: a correlation standard and clues to environmental history. Palaeogeogr. Palaeoclimatol. Palaeoecol. 294, 189–201. https://doi.org/10.1016/j.palaeo.2010.01.003.

Algeo, T.J., Luo, G.M., Song, H.Y., Lyons, T.W., Canfield, D.E., 2015. Reconstruction of secular variation in seawater sulfate concentrations. Biogeosciences 12, 2131–2151. https://doi.org/10.5194/bg-12-2131-2015.

Amend, J.P., Edwards, K.J., Lyons, T.W., 2004. Sulfur Biogeochemistry. The Geological Society of America (Special Papers).

Banner, J.L., Hanson, G.N., 1990. Calculation of simultaneous isotopic and trace element variations during water–rock interaction with applications to carbonate diagenesis. Geochim. Cosmochim. Acta 54, 3123–3137. https://doi.org/10.1016/0016-7037(90)90128-8.

Bergström, S.M., Carnes, J.B., 1985. Conodont Biostratigraphy of the Lower Middle Ordovician Chickamauga Group at Thorn Hill and Evans Ferry. pp. 51–60.

Bergström, S.M., Young, S., Schmitz, B., 2010. Katian (Upper Ordovician) $\delta^{13}C$ chemostratigraphy and sequence stratigraphy in the United States and Baltoscandia: a regional comparison. Palaeogeogr. Palaeoclimatol. Palaeoecol. 296, 217–234. https://doi.org/10.1016/j.palaeo.2010.02.035.

Bergström, S.M., Eriksson, M.E., Schmitz, B., Young, S.A., Ahlberg, P., 2016. Upper Ordovician $\delta^{13}C$ orgchemostratigraphy, K-bentonite stratigraphy, and biostratigraphy in southern Scandinavia: a reappraisal. Palaeogeogr. Palaeoclimatol. Palaeoecol. 454, 175–188. https://doi.org/10.1016/j.palaeo.2016.04.037.

Berner, R.A., 1985. Sulphate reductiom, organic matter decomposition and pyrite formation. Philos. Trans. R. Soc. Lond. 315, 25–38.

Berner, R.A., 2001. Modeling atmospheric O_2 over Phanerozoic time. Geochim. Cosmochim. Acta 65, 685–694. https://doi.org/10.1016/S0016-7037(00)00572-X.

Berner, R.A., 2004. The Phanerozoic Carbon Cycle: CO_2 and O_2. The Oxford University Press, New York.

Berner, R.A., 2006a. GEOCARBSULF: a combined model for Phanerozoic atmospheric O_2 and CO_2. Geochim. Cosmochim. Acta 70, 5653–5664. https://doi.org/10.1016/j.gca.2005.11.032.

Berner, R.A., 2006b. Inclusion of the weathering of volcanic rocks in the GEOCARBSULF model. Am. J. Sci. 306, 295–302.

Berner, R.A., Petsch, S.T., Lake, J.A., Beerling, D.J., Popp, B.N., Lane, R.S., Laws, E.A., Westley, M.B., Cassar, N., Woodward, F.I., Quick, W.P., 2000. Isotope fractionation and atmospheric oxygen: implications for Phanerozoic O_2 evolution. Science (New York, N.Y.) 287, 1630–1633. https://doi.org/10.1126/science.287.5458.1630.

Bidigare, R.R., Fluegge, A., Freeman, K., Hanson, K.L., Hayes, J.M., Hollander, D., Jasper, J.P., King, L.L., Laws, Edward A., Milder, J., Millero, F.J., Pancost, R.D., Popp, B.N., Steinberg, P.A., et al., 1997. Consistent Fractionation of ^{13}C in nature and in the laboratory: growth-rate effects in some haptophyte algae. Glob. Biogeochem. Cycles 11, 279–292. https://doi.org/10.1029/96GB03939.

Blakey, R.C., 2011. Middle Ordovician North American Paleogeographic Map. http://www2.nau.edu/rcb7/namO470.jpg.

Burdett, J.W., Arthur, M.A., Richardson, M., 1989. A Neogene seawater sulfur isotope age curve from calcareous pelagic microfossils. Earth Planet. Sci. Lett. 94, 189–198. https://doi.org/10.1016/0012-821X(89)90138-6.

Burke, A., Present, T.M., Paris, G., Rae, E.C.M., Sandilands, B.H., Gaillardet, J., Peucker-Ehrenbrink, B., Fischer, W.W., McClelland, J.W., Spencer, R.G.M., Voss, B.M., Adkins, J.F., 2018. Sulfur isotopes in rivers: Insights into global weathering budgets, pyrite oxidation, and the modern sulfur cycle. Earth Planet. Sci. Lett. 496, 168–177. https://doi.org/10.1016/j.epsl.2018.05.022.

Canfield, D.E., 2001. Biogeochemistry of sulfur isotopes. Rev. Mineral. Geochem. 43 (1), 607–636. https://doi.org/10.2138/gsrmg.43.1.607.

Canfield, D.E., Raiswell, R., Bottrell, S.H., 1992. The reactivity of sedimentary iron minerals towards sulfide. Am. J. Sci. 292, 659–683.

Canfield, D.E., Poulton, S.W., Narbonne, G.M., 2007. Late-Neoproterozoic deep-ocean oxygentation and the rise of animal life. Science 315, 92–94. https://doi.org/10.1126/science.1135013.

Cárdenas, A.L., Harries, P.J., 2010. Effect of nutrient availability on marine origination rates throughout the Phanerozoic eon. Nat. Geosci. 3, 430–434. https://doi.org/10.1038/ngeo869.

Carlucci, J.R., Westrop, S.R., Brett, C.E., Burkhalter, R., 2014. Facies architecture and sequence stratigraphy of the Ordovician Bromide Formation (Oklahoma): a new perspective on a mixed carbonate-siliciclastic ramp. Facies 60, 987–1012. https://doi.org/10.1007/s10347-014-0412-6.

Carnes, J.B., 1975. Conodont Biostratigraphy in the Lower-Middle Ordovician of the Western Appalachian Thrust Belts in Northeastern Tennessee. Ohio State University, pp. 76–994.

Chen, D., Wang, J., Racki, G., Li, H., Wang, C., Ma, X., Whalen, M.T., 2013. Large sulphur isotopic perturbations and oceanic changes during the Frasnian–Famennian transition of the Late Devonian. J. Geol. Soc. 170, 465–476. https://doi.org/10.1144/jgs2012-037.

Droser, M.L., Finnegan, S., 2003. The Ordovician radiation: a follow-up to the Cambrian explosion? Integr. Comp. Biol. 43, 178–184. https://doi.org/10.1093/icb/43.1.178.

Droser, M.L., Sheehan, P.M., 1997. Palaeoecology of the Ordovician radiation; resolution of large-scale patterns with individual clade histories, palaeogeography and environments. Geobios 30, 221–229. https://doi.org/10.1016/S0016-6995(97)80027-7.

Edwards, C.T., Saltzman, M.R., 2015. Paired carbon isotopic analysis of Ordovician bulk carbonate ($\delta^{13}C_{carb}$) and organic matter ($\delta^{13}C_{org}$) spanning the Great Ordovician Biodiversification Event. Palaeogeogr. Palaeoclimatol. Palaeoecol. 13. https://doi.org/10.1016/j.palaeo.2015.08.005.

Edwards, C.T., Saltzman, M.R., Royer, D.L., Fike, D.A., 2017. Oxygenation as a driver of the Great Ordovician Biodiversification Event. Nat. Geosci. 10, 925–929. https://doi.org/10.1038/s41561-017-0006-3.

Edwards, C.T., Fike, D.A., Saltzman, M.R., Lu, W., Lu, Z., 2018. Evidence for local and global redox conditions at an Early Ordovician (Tremadocian) mass extinction. Earth Planet. Sci. Lett. 481, 125–135. https://doi.org/10.1016/j.epsl.2017.10.002.

Ettensohn, F.R., Lierman, T.R., 2012. Large-scale tectonic controls on the origin of Paleozoic dark-shale source-rock basins: examples from the Appalachian Foreland Basin, Eastern United States. AAPG Bull. 100, 95–124. https://doi.org/10.1306/13351549M1003529.

Fike, D.A., Grotzinger, J.P., Pratt, L.M., Summons, R.E., 2006. Oxidation of the Ediacaran ocean. Nature 444, 744–747. https://doi.org/10.1038/nature05345.

Foland, K.A., Allen, J.C., 1991. Magma sources for Mesozoic anorogenic granites of the White Mountain magma series, New England, USA. Contrib. Mineral. Petrol. 109, 195–211. https://doi.org/10.1007/BF00306479.

Frakes, L.A., Francis, J.E., Syktus, J.I., 1992. Climate Modes of the Phanerozoic. Cambridge University Press, New York.

Gill, B.C., Lyons, T.W., Frank, T.D., 2008. Behavior of carbonate-associated sulfate during meteoric diagenesis and implications for the sulfur isotope paleoproxy. Geochim. Cosmochim. Acta 72, 4699–4711. https://doi.org/10.1016/j.gca.2008.07.001.

Gill, B.C., Lyons, T.W., Young, S.A., Kump, L.R., Knoll, A.H., Saltzman, M.R., 2011. Geochemical evidence for widespread euxinia in the later Cambrian ocean. Nature

469, 80–83. https://doi.org/10.1038/nature09700.
Gomes, M.L., Hurtgen, M.T., 2015. Sulfur isotope fractionation in modern euxinic systems: implications for paleoenvironmental reconstructions of paired sulfate-sulfide isotope records. Geochim. Cosmochim. Acta 157, 39–55. https://doi.org/10.1016/j.gca.2015.02.031.
Haq, B.U., Schutter, S.R., 2008. A chronology of Paleozoic sea-level changes. Science 322, 64–68. https://doi.org/10.1126/science.1161648.
Harper, D.A.T., Hammarlund, E.U., Rasmussen, C.M.Ø., 2014. End Ordovician extinctions: a coincidence of causes. Gondwana Res. 25, 1294–1307. https://doi.org/10.1016/j.gr.2012.12.021.
Hayes, J.M., Harald, S., Kaufman, A.J., 1999. The abundance of ^{13}C in marine organic matter and isotopic fractionation in the global biogeochemical cycle of carbon during the past 800 Ma. Chem. Geol. 161, 103–125. https://doi.org/10.1016/S0009-2541(99)00083-2.
Haynes, J.T., 1994. The Ordovician Deicke and Millbrig K-bentonite beds of the Cincinnati Arch and the Southern Valley and Ridge Province. Geol. Soc. Am. Spec. Pap. 290, 1–68.
Higgins, J.A., Blättler, C.L., Lundstrom, E.A., Santiago-Ramos, D.P., Akhtar, A.A., Crüger Ahm, A.S., Bialik, O., Holmden, C., Bradbury, H., Murray, S.T., Swart, P.K., 2018. Mineralogy, early marine diagenesis, and the chemistry of shallow-water carbonate sediments. Geochim. Cosmochim. Acta 220, 512–534. https://doi.org/10.1016/j.gca.2017.09.046.
Hurtgen, M.T., Halverson, G.P., Arthur, M.A., Hoffman, P.F., 2006. Sulfur cycling in the aftermath of a 635-Ma snowball glaciation: evidence for a syn-glacial sulfidic deep ocean. Earth Planet. Sci. Lett. 245, 551–570. https://doi.org/10.1016/j.epsl.2006.03.026.
Johnston, D.T., Poulton, S.W., Goldberg, T., Sergeev, V.N., Podkovyrov, V., Vorob'eva, N.G., Bekker, A., Knoll, A.H., 2012. Late Ediacaran redox stability and metazoan evolution. Earth Planet. Sci. Lett. 335–336, 25–35. https://doi.org/10.1016/j.epsl.2012.05.010.
Jones, D.S., Fike, D.A., 2013. Dynamic sulfur and carbon cycling through the end-Ordovician extinction revealed by paired sulfate–pyrite $\delta^{34}S$. Earth Planet. Sci. Lett. 363, 144–155. https://doi.org/10.1016/j.epsl.2012.12.015.
Kah, L.C., Lyons, T.W., Frank, T.D., 2004. Low marine sulphate and protracted oxygenation of the Proterozoic biosphere. Nature 431, 834–838. https://doi.org/10.1038/nature02974.
Knoll, A.H., Carroll, S.B., 1999. Animal Evolution: Biology Emerging Views From Comparative and Advancement of Science. 284. pp. 2129–2137. https://doi.org/10.1126/science.284.5423.2129.
Kolata, D.R., Huff, W.D., Bergström, S.M., 1996. Ordovician K-bentonites of Eastern North America. Geol. Soc. Am. Spec. Pap. 313, 1–76.
Korte, C., Kozur, H.W., Joachimski, M.M., Strauss, H., Veizer, J., Schwark, L., 2004. Carbon, sulfur, oxygen and strontium isotope records, organic geochemistry and biostratigraphy across the Permian/Triassic boundary in Abadeh, Iran. Int. J. Earth Sci. 93, 565–581. https://doi.org/10.1007/s00531-004-0406-7.
Kump, L.R., Arthur, M.A., 1999. Interpreting carbon-isotope excursions: carbonates and organic matter. Chem. Geol. 161, 181–198. https://doi.org/10.1016/S0009-2541(99)00086-8.
Kump, L.R., Garrels, R.M., 1986. Modeling atmospheric O_2 in the global sedimentary redox cycle. Am. J. Sci. 286, 337–360. https://doi.org/10.2475/ajs.286.5.337.
Kump, L.R., Arthur, M.A., Patzkowsky, M.E., Gibbs, M.T., Pinkus, D.S., Sheehan, P.M., 1999. A weathering hypothesis for glaciation at high atmospheric pCO_2 during the Late Ordovician. Palaeogeogr. Palaeoclimatol. Palaeoecol. 152, 173–187. https://doi.org/10.1016/S0031-0182(99)00046-2.
Kurtz, A.C., Kump, L.R., Arthur, M.A., Zachos, J.C., Paytan, A., 2003. Early Cenozoic decoupling of the global carbon and sulfur cycles. Paleoceanography 18. https://doi.org/10.1029/2003PA000908.
Leavitt, W.D., Halevy, I., Bradley, A.S., Johnston, D.T., 2013. Influence of sulfate reduction rates on the Phanerozoic sulfur isotope record. Proc. Natl. Acad. Sci. 110, 11244–11249. https://doi.org/10.1073/pnas.1218874110.
Lindskog, A., Costa, M.M., Rasmussen, C.M.Ø., Connelly, J.N., Eriksson, M.E., 2017. Refined Ordovician timescale reveals no link between asteroid breakup and biodiversification. Nat. Commun. 8, 14066. https://doi.org/10.1038/ncomms14066.
Lyons, T.W., Gill, B.C., 2010. Ancient sulfur cycling and oxygenation of the early biosphere. Elements 6, 93–99. https://doi.org/10.2113/gselements.6.2.93.
Marenco, P.J., Corsetti, F.a., Kaufman, A.J., Bottjer, D.J., 2008. Environmental and diagenetic variations in carbonate associated sulfate: an investigation of CAS in the Lower Triassic of the western USA. Geochim. Cosmochim. Acta 72, 1570–1582. https://doi.org/10.1016/j.gca.2007.10.033.
Marenco, P.J., Marenco, K.N., Lubitz, R.L., Niu, D., 2013. Contrasting long-term global and short-term local redox proxies during the Great Ordovician Biodiversification Event: a case study from Fossil Mountain, Utah, USA. Palaeogeogr. Palaeoclimatol. Palaeoecol. 377, 45–51. https://doi.org/10.1016/j.palaeo.2013.03.007.
Metzger, G.J., Fike, D.A., 2013. Techniques for assessing spatial heterogeneity of carbonate $\delta^{13}C$ values: implications for craton-wide isotope gradients. Sedimentology 60, 1405–1431. https://doi.org/10.1111/sed.12033.
Meyers, P.A., 1994. Preservation of elemental and isotopic source identification of sedimentary organic matter. Chem. Geol. 114, 289–302. https://doi.org/10.1016/0009-2541(94)90059-0.
Miller, A.I., Mao, S., 1995. Association of orogenic activity with the Ordovician radiation of marine life. Geology 23, 305–308. https://doi.org/10.1130/0091-7613(1995)023<0305:AOOAWT>2.3.CO.
Mitterer, R.M., 2010. Methanogenesis and sulfate reduction in marine sediments: a new model. Earth Planet. Sci. Lett. 295, 358–366. https://doi.org/10.1016/j.epsl.2010.04.009.
Munnecke, A., Calner, M., Harper, D.A.T., Servais, T., 2010. Ordovician and Silurian seawater chemistry, sea level, and climate: a synopsis. Palaeogeogr. Palaeoclimatol. Palaeoecol. 296, 389–413. https://doi.org/10.1016/j.palaeo.2010.08.001.
Mussman, W.J., Read, J.F., 1986. Sedimentology and development of a passive- to convergent-margin unconformity: Middle Ordovician Knos unconformity, Virginia Appalachians. Geol. Soc. Am. Bull. 97 (282–295), 282–295.
Nielsen, A.T., 2004. Ordovician sea level changes: a Baltoscandian perspective. In: Webby, B.D., Paris, F., Droser, M.L., Percival, I.G. (Eds.), The Great Ordovician Biodiversification Event. Columbia Press, New York, pp. 84–93.
Oehlert, A.M., Swart, P.K., 2014. Interpreting carbonate and organic carbon isotope covariance in the sedimentary record. Nat. Commun. 5, 4672. https://doi.org/10.1038/ncomms5672.
Owens, J.D., Gill, B.C., Jenkyns, H.C., Bates, S.M., Severmann, S., Kuypers, M.M.M., Woodfine, R.G., Lyons, T.W., 2013. Sulfur isotopes track the global extent and dynamics of euxinia during Cretaceous Oceanic Anoxic Event 2. Proc. Natl. Acad. Sci. 110, 18407–18412. https://doi.org/10.1073/pnas.1305304110.
Panchuk, K.M., Holmden, C., Kump, L.R., 2005. Sensitivity of the epeiric sea carbon isotope record to local-scale carbon cycle processes: tales from the Mohawkian Sea. Palaeogeogr. Palaeoclimatol. Palaeoecol. 228, 320–337. https://doi.org/10.1016/j.palaeo.2005.06.019.
Peng, Y., Bao, H., Pratt, L.M., Kaufman, A.J., Jiang, G., Boyd, D., Wang, Q., Zhou, C., Yuan, X., Xiao, S., Loyd, S., 2014. Widespread contamination of carbonate-associated sulfate by present-day secondary atmospheric sulfate: Evidence from triple oxygen isotopes. Geology 42, 815–818. https://doi.org/10.1130/G35852.1.
Peters, S.E., 2004. Evenness of Cambrian – Ordovician benthic marine communities in North America Evenness of Cambrian – Ordovician benthic marine communities in North America. Paleobiology 30, 325–346.
Pope, M., Read, J.F., 1998. Ordovician metre-scale cycles: implications for climate and eustatic fluctuations in the central Appalachians during a global greenhouse, non-glacial to glacial transition. Palaeogeogr. Palaeoclimatol. Palaeoecol. 138, 27–42. https://doi.org/10.1016/S0031-0182(97)00130-2.
Popp, B.N., Laws, E.A., Bridigare, R.R., Dore, J.E., Hanson, K.L., Wakeham, S.G., 1998. Effect of phytplankton cell geometry on carbon isotopis fractionation. Geochim. Cosmochim. Acta 62, 69–77.
Present, T.M., Paris, G., Burke, A., Fischer, W.W., Adkins, J.F., 2015. Large Carbonate Associated Sulfate isotopic variability between brachiopods, micrite, and other sedimentary components in Late Ordovician strata. Earth Planet. Sci. Lett. 432, 187–198. https://doi.org/10.1016/j.epsl.2015.10.005.
Rasmussen, C.M.Ø., Ullmann, C.V., Jakobsen, K.G., Lindskog, A., Hansen, J., Hansen, T., Eriksson, M.E., Dronov, A., Frei, R., Korte, C., Nielsen, A.T., Harper, D.A.T., 2016. Onset of main Phanerozoic marine radiation sparked by emerging Mid Ordovician icehouse. Sci. Rep. 6, 18884. https://doi.org/10.1038/srep18884.
Saltzman, M.R., 2005. Phosphorus, nitrogen, and the redox evolution of the Paleozoic oceans. Geology 33, 573–576. https://doi.org/10.1130/G21535.1.
Saltzman, M.R., Edwards, C.T., 2017. Gradients in the carbon isotopic composition of Ordovician shallow water carbonates: a potential pitfall in estimates of ancient CO_2 and O_2. Earth Planet. Sci. Lett. 464, 46–54. https://doi.org/10.1016/j.epsl.2017.02.011.
Saltzman, M.R., Young, S.A., Kump, L.R., Gill, B.C., Lyons, T.W., Runnegar, B., 2011. Pulse of atmospheric oxygen during the late Cambrian. Proc. Natl. Acad. Sci. U. S. A. 108, 3876–3881. https://doi.org/10.1073/pnas.1011836108.
Saltzman, M.R., Edwards, C.T., Leslie, S.A., Dwyer, G.S., Bauer, J.A., Repetski, J.E., Harris, A.G., Bergström, S.M., 2014. Calibration of a conodont apatite-based Ordovician $^{87}Sr/^{86}Sr$ curve to biostratigraphy and geochronology: implications for stratigraphic resolution. Bull. Geol. Soc. Am. 126, 1551–1568. https://doi.org/10.1130/B31038.1.
Saltzman, M.R., Edwards, C.T., Adrain, J.M., Westrop, S.R., 2015. Persistent oceanic anoxia and elevated extinction rates separate the Cambrian and Ordovician radiations. Geology 43, G36814.1. https://doi.org/10.1130/G36814.1.
Schmitz, B., Harper, D.A.T., Peucker-Ehrenbrink, B., Stouge, S., Alwmark, C., Cronholm, A., Bergström, S.M., Tassinari, M., Xiaofeng, W., 2008. Asteroid breakup linked to the Great Ordovician Biodiversification Event. Nat. Geosci. 1, 49–53. https://doi.org/10.1038/ngeo.2007.37.
Sepkoski, J.J., Bambach, R.K., Raup, D.M., Valentine, J.W., 1981. Phanerozoic marine diversity and the fossil record. Nature 293, 435–437. https://doi.org/10.1038/293435a0.
Servais, T., Owen, A.W., Harper, D.A.T., Kröger, B., Munnecke, A., 2010. The Great Ordovician Biodiversification Event (GOBE): the palaeoecological dimension. Palaeogeogr. Palaeoclimatol. Palaeoecol. 294, 99–119. https://doi.org/10.1016/j.palaeo.2010.05.031.
Shen, B., Xiao, S., Kaufman, A.J., Bao, H., Zhou, C., Wang, H., 2008. Stratification and mixing of a post-glacial Neoproterozoic ocean: evidence from carbon and sulfur isotopes in a cap dolostone from northwest China. Earth Planet. Sci. Lett. 265, 209–228. https://doi.org/10.1016/j.epsl.2007.10.005.
Sim, M.S., Bosak, T., Ono, S., 2011a. Large sulfur isotope fractionation does not require disproportionation. Science 333, 74–77.
Sim, M.S., Ono, S., Donovan, K., Templer, S.P., Bosak, T., 2011b. Effect of electron donors on the fractionation of sulfur isotopes by a marine Desulfovibrio sp. Geochim. Cosmochim. Acta 75, 4244–4259. https://doi.org/10.1016/j.gca.2011.05.021.
Sim, M.S., Ono, S., Hurtgen, M.T., 2015. Sulfur isotope evidence for low and fluctuating sulfate levels in the Late Devonian ocean and the potential link with the mass extinction event. Earth Planet. Sci. Lett. 419, 52–62. https://doi.org/10.1016/j.epsl.2015.03.009.
Sperling, E.A., Frieder, C.A., Raman, A.V., Girguis, P.R., Levin, L.A., Knoll, A.H., 2013. Oxygen, ecology, and the Cambrian radiation of animals. Proc. Natl. Acad. Sci. 110, 13446–13451. https://doi.org/10.1073/pnas.1312778110.
Stanley, S.M., 1973. An ecological theory for the sudden origin of multicelluar life in the

Late Precambrian. Proc. Natl. Acad. Sci. 70, 1486–1489.
Swanson-Hysell, N.L., Macdonald, F.A., 2017. Tropical weathering of the Taconic orogeny as a driver for Ordovician cooling. Geology 45 (8), 719–722. https://doi.org/10.1130/G38985.1.
Swart, P.K., Oehlert, A.M., 2018. Revised interpretations of stable C and O patters in carbonate rocks resulting from meteoric diagenesis. Sediment. Geol. 364, 14–23. https://doi.org/10.1016/j.sedgeo.2017.12.005.
Thompson, C.K., Kah, L.C., 2012. Sulfur isotope evidence for widespread euxinia and a fluctuating oxycline in Early to Middle Ordovician greenhouse oceans. Palaeogeogr. Palaeoclimatol. Palaeoecol. 313–314, 189–214. https://doi.org/10.1016/j.palaeo.2011.10.020.
Thompson, C.K., Kah, L.C., Astini, R., Bowring, S.a., Buchwaldt, R., 2012. Bentonite geochronology, marine geochemistry, and the Great Ordovician Biodiversification Event (GOBE). Palaeogeogr. Palaeoclimatol. Palaeoecol. 321–322, 88–101. https://doi.org/10.1016/j.palaeo.2012.01.022.
Trotter, J.A., Williams, I.S., Barnes, C.R., Lécuyer, C., Nicoll, R.S., 2008. Did cooling oceans trigger Orovician biodiversification? Evidence from conodont thermometry. Science 321, 550–554. https://doi.org/10.1126/science.1155814.
Vail, P.R., Mitchum, R.M., Thompson, S., 1977. Seismic stratigraphy and global changes of sea level: part 3. Relative changes of sea level from Coastal Onlap: section 2. Application of seismic reflection configuration to stratigraphic interpretation. AAPG Spec. Vol. 165, 63–81.
Wildman, R.A., Berner, R.A., Petsch, S.T., Bolton, E.W., Eckert, J.O., Mok, U., Evans, J.B., 2004. The weathering of sedimentary organic matter as a control on atsmospheric O_2: I. Analysis of a black shale. Am. J. Sci. 304, 234–249. https://doi.org/10.2475/ajs.304.3.234.
Wotte, T., Shields-Zhou, G.A., Strauss, H., 2012. Carbonate-associated sulfate: experimental comparisons of common extraction methods and recommendations toward a standard analytical protocol. Chem. Geol. 326–327, 132–144. https://doi.org/10.1016/j.chemgeo.2012.07.020.
Young, S.A., Saltzman, M.R., Bergström, S.M., Leslie, S.A., Xu, C., 2008. Paired $\delta^{13}C_{carb}$ and $\delta^{13}C_{org}$ records of Upper Ordovician (Sandbian-Katian) carbonates in North America and China: implications for paleoceanographic change. Palaeogeogr. Palaeoclimatol. Palaeoecol. 270, 166–178. https://doi.org/10.1016/j.palaeo.2008.09.006.
Young, S.a., Saltzman, M.R., Foland, K.a., Linder, J.S., Kump, L.R., 2009. A major drop in seawater $^{87}Sr/^{86}Sr$ during the Middle Ordovician (Darriwilian): links to volcanism and climate? Geology 37, 951–954. https://doi.org/10.1130/G30152A.1.
Young, S.A., Gill, B.C., Edwards, C.T., Saltzman, M.R., Leslie, S.A., 2016. Middle–Late Ordovician (Darriwilian–Sandbian) decoupling of global sulfur and carbon cycles: Isotopic evidence from eastern and southern Laurentia. Palaeogeogr. Palaeoclimatol. Palaeoecol. https://doi.org/10.1016/j.palaeo.2015.09.040.